

Effect of non-uniform efficiency on the measurement of higher-order cumulants in heavy-ion collisions

Fan Si,¹ Yifei Zhang,^{1,*} and Xiaofeng Luo^{2,†}

¹*State Key Laboratory of Particle Detection and Electronics,
University of Science and Technology of China, Hefei 230026, China*

²*Key Laboratory of Quark & Lepton Physics (MOE) and Institute of Particle Physics,
Central China Normal University, Wuhan 430079, China*

(Dated: March 25, 2022)

We perform a systematic study for the effect of non-uniform track efficiency on the efficiency correction of higher-order cumulant analysis in heavy-ion collisions. Through analytical derivation, we find that the true values of cumulants can be successfully reproduced by the efficiency correction with an average of the realistic detector efficiency for particles with the same charges within each single phase space. However, with taking an average across multiple phase spaces or introducing a non-averaged distribution, the efficiency correction for higher-order cumulants becomes invalid accordingly. During a toy model simulation by tuning the non-uniformity of the efficiency employed in the track-by-track efficiency correction method, the theoretical conclusions are supported and the valid averaged efficiency with less non-uniformity is found to suppress the statistical uncertainties of the reproduced cumulants dramatically. Thus, the usage of averaged efficiency requires a careful study for the phase space dependence. This study is important for carrying out precise measurement of higher-order cumulants for various detector acceptance in heavy-ion collision experiments at present and in future.

I. INTRODUCTION

In nature, quarks and gluons are confined in the nucleons by the strong interaction. In the extremely hot and dense condition created in relativistic heavy-ion collisions, those partons can be liberated via deconfinement to form Quark-Gluon Plasma (QGP) [1, 2], which is believed to exist in the early universe around tens of microseconds after the Big Bang. Many experimental evidences show that the QGP is strongly coupled and behaves like a perfect liquid [3–9]. The Quantum Chromodynamics (QCD) predicts that at large temperature (T) and small baryon chemical potential (μ_B), it is a smooth crossover from hadronic phase to partonic phase [10]. While at relatively smaller T and larger μ_B , QCD-based models predict a first-order phase transition between these two phases [11–13]. Thus, there should be a critical point (CP) connecting the crossover region and first-order phase transition line. One of the most important goals of heavy-ion collisions is to search for the possible QCD critical point in the QCD phase diagram with sensitive observables [14–17].

Higher-order cumulants of conserved charges, such as net-baryon (B), net-charge (Q) and net-strangeness (S), are proposed as sensitive observables to search for the QCD critical point in heavy-ion collisions [18–23]. In the first phase of the RHIC Beam Energy Scan program (BES-I, 2010–2017), experimentally measured fourth-order net-proton fluctuations ($\kappa\sigma^2$) in 0–5% central Au+Au collisions show a non-monotonic energy dependence with a 3.1σ significance [24–27]. However, due

to limited event statistics, the statistical uncertainties are still large below $\sqrt{s_{\text{NN}}} = 20$ GeV. To confirm the intriguing observation in BES-I, the STAR experiment has conducted the second phase of the Beam Energy Scan program (BES-II) since 2019, which is focusing on the energies below $\sqrt{s_{\text{NN}}} = 20$ GeV and with 10–20 times more than the statistics collected in BES-I. In the data analysis, the statistical uncertainties of higher-order cumulants are not only determined by the event statistics, but also depending on the particle detecting efficiency and acceptance [28–30]. In a previous study, a track-by-track-based method has been developed to apply the efficiency correction in the higher-order cumulant analysis of conserved charges [31]. In this paper, we further investigate the effect of non-uniformity of the detector efficiency/acceptance on the efficiency correction, which is important to perform precise measurement of higher-order cumulants for various detector acceptance in future heavy-ion collisions experiments.

II. THEORETICAL STUDY

In heavy-ion collisions, the particle detection efficiency is usually non-uniform and could depend on many factors, such as the collision centrality, track kinematic parameters (transverse momentum p_T , azimuth angle φ and rapidity y) and track crossing effect [32]. In data analysis, the efficiency is usually employed as its average within one or two wide phase spaces (so-called bin-by-bin efficiency) [25, 33, 34], rather than a non-uniform distribution in various dimensions. For example, the detector acceptance in azimuth can be non-uniform due to dead areas or bad electronic readout channels.

In this section, a theoretical study is performed for

* ephy@ustc.edu.cn

† xfluo@ccnu.edu.cn

the validity of applying the efficiency employed in the correction (ε_c) with the same averaged value and different non-uniformity according to the detector efficiency in the measurement (ε_m) during the higher-order cumulant analysis of conserved charges.

A. Quantity definitions

In an event of heavy-ion collisions, there may be several phase spaces in which the particles are produced through different physical effects whose multiplicities are determined according to a certain joint distribution. For example, two phase spaces are considered with two series of particles with the multiplicities X and Y as non-negative integer random variables following the probability distribution function $P(X, Y)$. Note that there may be various types of particles with different charges belonging to a series produced in a phase space. The linear combination of X and Y with the coefficients a and b can be expressed by

$$Q_{(a,b)} = aX + bY, \quad (1)$$

The cumulants and factorial cumulants of $Q_{(a,b)}$ are given by [35, 36]

$$\left\langle Q_{(a,b)}^k Q_{(a',b')}^l \right\rangle_c = \partial_{(a,b)}^k \partial_{(a',b')}^l K(\theta, \eta) \Big|_{\theta=\eta=0}, \quad (2)$$

$$\left\langle Q_{(a,b)}^k Q_{(a',b')}^l \right\rangle_{fc} = \bar{\partial}_{(a,b)}^k \bar{\partial}_{(a',b')}^l K_f(s, t) \Big|_{s=t=1} \quad (3)$$

from the generating functions

$$K(\theta, \eta) = \ln \sum_{X,Y} P(X, Y) e^{\theta X + \eta Y}, \quad (4)$$

$$K_f(s, t) = \ln \sum_{X,Y} P(X, Y) s^X t^Y \quad (5)$$

with

$$\partial_{(a,b)} = a \frac{\partial}{\partial \theta} + b \frac{\partial}{\partial \eta}, \quad (6)$$

$$\bar{\partial}_{(a,b)} = a \frac{\partial}{\partial s} + b \frac{\partial}{\partial t}. \quad (7)$$

The relation between cumulants and factorial cumulants is derived in Ref. [35].

The two phase spaces are divided into M and N bins, respectively, for example, according to the particle types and kinematic parameters. A single particle is allocated into various bins with the probability vector $\mathbf{p} = (p_1, p_2, \dots, p_M)$ or $\mathbf{q} = (q_1, q_2, \dots, q_N)$, which can be determined by the distributions of p_T , φ and y of different types of particles. Thus, the bin-by-bin particle numbers, represented by the vectors $\mathbf{X} = (X_1, X_2, \dots, X_M)$ and $\mathbf{Y} = (Y_1, Y_2, \dots, Y_N)$, follow the probability distribution function

$$\tilde{P}(\mathbf{X}, \mathbf{Y}) = \sum_{X,Y} P(X, Y) \mathcal{M}_{X,\mathbf{p}}(\mathbf{X}) \mathcal{M}_{Y,\mathbf{q}}(\mathbf{Y}), \quad (8)$$

where $\mathcal{M}_{X,\mathbf{p}}(\mathbf{X})$ and $\mathcal{M}_{Y,\mathbf{q}}(\mathbf{Y})$ denote the multinomial distributions defined as

$$\mathcal{M}_{X,\mathbf{p}}(\mathbf{X}) = \frac{X!}{\prod_{i=1}^M X_i!} \prod_{i=1}^M p_i^{X_i} \quad (9)$$

with $\sum_{i=1}^M X_i = X$ and $\sum_{i=1}^M p_i = 1$. The linear combination of the bin-by-bin particle numbers with the coefficients $\mathbf{a} = (a_1, a_2, \dots, a_M)$ and $\mathbf{b} = (b_1, b_2, \dots, b_N)$ and its cumulants and factorial cumulants are given by

$$Q_{(\mathbf{a},\mathbf{b})} = \mathbf{a} \cdot \mathbf{X} + \mathbf{b} \cdot \mathbf{Y}, \quad (10)$$

$$\left\langle Q_{(\mathbf{a},\mathbf{b})}^k Q_{(\mathbf{a}',\mathbf{b}')}^l \right\rangle_c = \partial_{(\mathbf{a},\mathbf{b})}^k \partial_{(\mathbf{a}',\mathbf{b}')}^l \tilde{K}(\theta, \eta) \Big|_{\theta=\eta=0}, \quad (11)$$

$$\left\langle Q_{(\mathbf{a},\mathbf{b})}^k Q_{(\mathbf{a}',\mathbf{b}')}^l \right\rangle_{fc} = \bar{\partial}_{(\mathbf{a},\mathbf{b})}^k \bar{\partial}_{(\mathbf{a}',\mathbf{b}')}^l \tilde{K}_f(s, t) \Big|_{s=t=1} \quad (12)$$

from the generating functions

$$\tilde{K}(\theta, \eta) = \ln \sum_{\mathbf{X}, \mathbf{Y}} \tilde{P}(\mathbf{X}, \mathbf{Y}) e^{\theta \cdot \mathbf{X} + \eta \cdot \mathbf{Y}}, \quad (13)$$

$$\tilde{K}_f(s, t) = \ln \sum_{\mathbf{X}, \mathbf{Y}} \tilde{P}(\mathbf{X}, \mathbf{Y}) \prod_{i=1}^M s_i^{X_i} \prod_{j=1}^N t_j^{Y_j} \quad (14)$$

with

$$\partial_{(\mathbf{a},\mathbf{b})} = \sum_{i=1}^M a_i \frac{\partial}{\partial \theta_i} + \sum_{j=1}^N b_j \frac{\partial}{\partial \eta_j}, \quad (15)$$

$$\bar{\partial}_{(\mathbf{a},\mathbf{b})} = \sum_{i=1}^M a_i \frac{\partial}{\partial s_i} + \sum_{j=1}^N b_j \frac{\partial}{\partial t_j}. \quad (16)$$

The $Q_{(\mathbf{a},\mathbf{b})}$ gives the conserved charge in the collision system if \mathbf{a} and \mathbf{b} denote two series of particle charges in various bins, respectively. For two series of particles with the same charges $a_i \equiv a$ ($i = 1, 2, \dots, M$) and $b_j \equiv b$ ($j = 1, 2, \dots, N$), $Q_{(\mathbf{a},\mathbf{b})} = Q_{(a,b)}$. The k th-order diagonal cumulant $\left\langle Q_{(a,b)}^k \right\rangle_c$ can be simply marked by C_k .

The $\tilde{K}_f(s, t)$ can be converted into $K_f(s, t)$ with

$$\begin{aligned} \tilde{K}_f(s, t) &= \ln \sum_{X,Y} P(X, Y) \sum_{\mathbf{X}} \mathcal{M}_{X,\mathbf{p}}(\mathbf{X}) \prod_{i=1}^M s_i^{X_i} \\ &\quad \times \sum_{\mathbf{Y}} \mathcal{M}_{Y,\mathbf{q}}(\mathbf{Y}) \prod_{j=1}^N t_j^{Y_j} \\ &= \ln \sum_{X,Y} P(X, Y) \left(\sum_{i=1}^M p_i s_i \right)^X \left(\sum_{j=1}^N q_j t_j \right)^Y \\ &= K_f \left(\sum_{i=1}^M p_i s_i, \sum_{j=1}^N q_j t_j \right), \end{aligned} \quad (17)$$

where the third line is obtained by the multinomial expansion, so

$$\bar{\partial}_{(\mathbf{a}, \mathbf{b})}^k \bar{\partial}_{(\mathbf{a}', \mathbf{b}')}^l \tilde{K}_{\mathbf{f}}(\mathbf{s}, \mathbf{t}) = \bar{\partial}_{(\mathbf{a} \cdot \mathbf{p}, \mathbf{b} \cdot \mathbf{q})}^k \bar{\partial}_{(\mathbf{a}' \cdot \mathbf{p}, \mathbf{b}' \cdot \mathbf{q})}^l K_{\mathbf{f}}(s, t). \quad (18)$$

Now the detector efficiency is taken into consideration. A single particle in each bin is detected independently with the probability vector $\boldsymbol{\alpha} = (\alpha_1, \alpha_2, \dots, \alpha_M)$ or $\boldsymbol{\beta} = (\beta_1, \beta_2, \dots, \beta_N)$. As a result, the probability distribution function of the measured bin-by-bin particle numbers $\mathbf{x} = (x_1, x_2, \dots, x_M)$ and $\mathbf{y} = (y_1, y_2, \dots, y_N)$ can be expressed by

$$\tilde{P}(\mathbf{x}, \mathbf{y}) = \sum_{\mathbf{X}, \mathbf{Y}} \tilde{P}(\mathbf{X}, \mathbf{Y}) \prod_{i=1}^M \mathcal{B}_{X_i, \alpha_i}(x_i) \prod_{j=1}^N \mathcal{B}_{Y_j, \beta_j}(y_j), \quad (19)$$

where $\mathcal{B}_{X_i, \alpha_i}(x_i)$ and $\mathcal{B}_{Y_j, \beta_j}(y_j)$ denote the binomial distributions defined by

$$\mathcal{B}_{X_i, \alpha_i}(x_i) = \frac{X_i!}{x_i!(X_i - x_i)!} \alpha_i^{x_i} (1 - \alpha_i)^{X_i - x_i} \quad (20)$$

as the binomial case of the multinomial distribution. The linear combination of the measured bin-by-bin particle numbers and its cumulants and factorial cumulants are given by

$$q_{(\mathbf{a}, \mathbf{b})} = \mathbf{a} \cdot \mathbf{x} + \mathbf{b} \cdot \mathbf{y}, \quad (21)$$

$$\left\langle q_{(\mathbf{a}, \mathbf{b})}^k q_{(\mathbf{a}', \mathbf{b}')}^l \right\rangle_c = \partial_{(\mathbf{a}, \mathbf{b})}^k \partial_{(\mathbf{a}', \mathbf{b}')}^l \tilde{K}(\boldsymbol{\theta}, \boldsymbol{\eta}) \Big|_{\boldsymbol{\theta}=\boldsymbol{\eta}=0}, \quad (22)$$

$$\left\langle q_{(\mathbf{a}, \mathbf{b})}^k q_{(\mathbf{a}', \mathbf{b}')}^l \right\rangle_{\text{fc}} = \bar{\partial}_{(\mathbf{a}, \mathbf{b})}^k \bar{\partial}_{(\mathbf{a}', \mathbf{b}')}^l \tilde{K}_{\mathbf{f}}(\mathbf{s}, \mathbf{t}) \Big|_{\mathbf{s}=\mathbf{t}=1} \quad (23)$$

from the generating functions

$$\tilde{K}(\boldsymbol{\theta}, \boldsymbol{\eta}) = \ln \sum_{\mathbf{x}, \mathbf{y}} \tilde{P}(\mathbf{x}, \mathbf{y}) e^{\boldsymbol{\theta} \cdot \mathbf{x} + \boldsymbol{\eta} \cdot \mathbf{y}}, \quad (24)$$

$$\tilde{K}_{\mathbf{f}}(\mathbf{s}, \mathbf{t}) = \ln \sum_{\mathbf{x}, \mathbf{y}} \tilde{P}(\mathbf{x}, \mathbf{y}) \prod_{i=1}^M s_i^{x_i} \prod_{j=1}^N t_j^{y_j}. \quad (25)$$

The relation between $\tilde{K}_{\mathbf{f}}(\mathbf{s}, \mathbf{t})$ and $\tilde{K}_{\mathbf{f}}(\mathbf{s}, \mathbf{t})$ can be derived by

$$\begin{aligned} \tilde{K}_{\mathbf{f}}(\mathbf{s}, \mathbf{t}) &= \ln \sum_{\mathbf{X}, \mathbf{Y}} \tilde{P}(\mathbf{X}, \mathbf{Y}) \sum_{\mathbf{x}} \prod_{i=1}^M \mathcal{B}_{X_i, \alpha_i}(x_i) s_i^{x_i} \\ &\quad \times \sum_{\mathbf{y}} \prod_{j=1}^N \mathcal{B}_{Y_j, \beta_j}(y_j) t_j^{y_j} \\ &= \ln \sum_{\mathbf{X}, \mathbf{Y}} \tilde{P}(\mathbf{X}, \mathbf{Y}) \prod_{i=1}^M (\alpha_i s_i + (1 - \alpha_i))^{X_i} \\ &\quad \times \prod_{j=1}^N (\beta_j t_j + (1 - \beta_j))^{Y_j} \\ &= \tilde{K}_{\mathbf{f}}(\mathbf{s}', \mathbf{t}'), \end{aligned} \quad (26)$$

where $s'_i = \alpha_i s_i + (1 - \alpha_i)$ ($i = 1, 2, \dots, M$) and $t'_j = \beta_j t_j + (1 - \beta_j)$ ($j = 1, 2, \dots, N$), so

$$\bar{\partial}_{(\mathbf{a}, \mathbf{b})}^k \bar{\partial}_{(\mathbf{a}', \mathbf{b}')}^l \tilde{K}_{\mathbf{f}}(\mathbf{s}, \mathbf{t}) = \bar{\partial}_{(\mathbf{a}\boldsymbol{\alpha}, \mathbf{b}\boldsymbol{\beta})}^k \bar{\partial}_{(\mathbf{a}'\boldsymbol{\alpha}, \mathbf{b}'\boldsymbol{\beta})}^l \tilde{K}_{\mathbf{f}}(\mathbf{s}, \mathbf{t}). \quad (27)$$

Here defines the expression

$$\bar{\partial}_{(\mathbf{a}\boldsymbol{\alpha}/\mathbf{a}', \mathbf{b}\boldsymbol{\beta}/\mathbf{b}')} = \sum_{i=1}^M \frac{a_i \alpha_i}{\alpha'_i} \frac{\partial}{\partial s_i} + \sum_{j=1}^N \frac{b_j \beta_j}{\beta'_j} \frac{\partial}{\partial t_j}, \quad (28)$$

which is similar to $Q_{(\mathbf{a}\boldsymbol{\alpha}/\mathbf{a}', \mathbf{b}\boldsymbol{\beta}/\mathbf{b}')}$, $q_{(\mathbf{a}\boldsymbol{\alpha}/\mathbf{a}', \mathbf{b}\boldsymbol{\beta}/\mathbf{b}')}$ and $\partial_{(\mathbf{a}\boldsymbol{\alpha}/\mathbf{a}', \mathbf{b}\boldsymbol{\beta}/\mathbf{b}')}$.

In the efficiency correction by using the true detector efficiency, the relations between the true $\left\langle Q_{(\mathbf{a}, \mathbf{b})}^k Q_{(\mathbf{a}', \mathbf{b}')}^l \right\rangle_c$ and the measured $\left\langle q_{(\mathbf{a}, \mathbf{b})}^k q_{(\mathbf{a}', \mathbf{b}')}^l \right\rangle_c$ are derived by three steps:

$$\begin{aligned} \left\langle Q_{(\mathbf{a}, \mathbf{b})}^k Q_{(\mathbf{a}', \mathbf{b}')}^l \right\rangle_c &\leftrightarrow \left\langle Q_{(\mathbf{a}, \mathbf{b})}^k Q_{(\mathbf{a}', \mathbf{b}')}^l \right\rangle_{\text{fc}} \\ &\quad \downarrow \\ \left\langle q_{(\mathbf{a}, \mathbf{b})}^k q_{(\mathbf{a}', \mathbf{b}')}^l \right\rangle_c &\leftrightarrow \left\langle q_{(\mathbf{a}, \mathbf{b})}^k q_{(\mathbf{a}', \mathbf{b}')}^l \right\rangle_{\text{fc}} \end{aligned}$$

For example, the true diagonal cumulants (C_k^{true}) up to third-order can be obtained from [35, 36]

$$C_1^{\text{true}} = \left\langle Q_{(\mathbf{a}, \mathbf{b})} \right\rangle_c = \left\langle Q_{(\mathbf{a}, \mathbf{b})} \right\rangle_{\text{fc}} = \left\langle q_{(\mathbf{a}/\mathbf{a}, \mathbf{b}/\mathbf{b})} \right\rangle_{\text{fc}} = \left\langle q_{(\mathbf{a}/\mathbf{a}, \mathbf{b}/\mathbf{b})} \right\rangle_c = C_1^{\text{corr}}(\boldsymbol{\alpha}, \boldsymbol{\beta}; \boldsymbol{\alpha}, \boldsymbol{\beta}), \quad (29)$$

$$\begin{aligned} C_2^{\text{true}} &= \left\langle Q_{(\mathbf{a}, \mathbf{b})}^2 \right\rangle_c = \left\langle Q_{(\mathbf{a}, \mathbf{b})}^2 \right\rangle_{\text{fc}} + \left\langle Q_{(\mathbf{a}^2, \mathbf{b}^2)} \right\rangle_{\text{fc}} = \left\langle q_{(\mathbf{a}/\mathbf{a}, \mathbf{b}/\mathbf{b})}^2 \right\rangle_{\text{fc}} + \left\langle q_{(\mathbf{a}^2/\mathbf{a}^2, \mathbf{b}^2/\mathbf{b}^2)} \right\rangle_{\text{fc}} \\ &= \left\langle q_{(\mathbf{a}/\mathbf{a}, \mathbf{b}/\mathbf{b})}^2 \right\rangle_c - \left\langle q_{(\mathbf{a}^2/\mathbf{a}^2, \mathbf{b}^2/\mathbf{b}^2)} \right\rangle_c + \left\langle q_{(\mathbf{a}^2/\mathbf{a}^2, \mathbf{b}^2/\mathbf{b}^2)} \right\rangle_c = C_2^{\text{corr}}(\boldsymbol{\alpha}, \boldsymbol{\beta}; \boldsymbol{\alpha}, \boldsymbol{\beta}), \end{aligned} \quad (30)$$

$$\begin{aligned} C_3^{\text{true}} &= \left\langle Q_{(\mathbf{a}, \mathbf{b})}^3 \right\rangle_c = \left\langle Q_{(\mathbf{a}, \mathbf{b})}^3 \right\rangle_{\text{fc}} + 3 \left\langle Q_{(\mathbf{a}, \mathbf{b})} Q_{(\mathbf{a}^2, \mathbf{b}^2)} \right\rangle_{\text{fc}} + \left\langle Q_{(\mathbf{a}^3, \mathbf{b}^3)} \right\rangle_{\text{fc}} \\ &= \left\langle q_{(\mathbf{a}/\mathbf{a}, \mathbf{b}/\mathbf{b})}^3 \right\rangle_c + 3 \left\langle q_{(\mathbf{a}/\mathbf{a}, \mathbf{b}/\mathbf{b})} q_{(\mathbf{a}^2/\mathbf{a}, \mathbf{b}^2/\mathbf{b}^2)} \right\rangle_{\text{fc}} + \left\langle q_{(\mathbf{a}^3/\mathbf{a}^3, \mathbf{b}^3/\mathbf{b}^3)} \right\rangle_{\text{fc}} \\ &= \left\langle q_{(\mathbf{a}/\mathbf{a}, \mathbf{b}/\mathbf{b})}^3 \right\rangle_c - 3 \left\langle q_{(\mathbf{a}/\mathbf{a}, \mathbf{b}/\mathbf{b})} q_{(\mathbf{a}^2/\mathbf{a}^2, \mathbf{b}^2/\mathbf{b}^2)} \right\rangle_c + 2 \left\langle q_{(\mathbf{a}^3/\mathbf{a}^3, \mathbf{b}^3/\mathbf{b}^3)} \right\rangle_c \\ &\quad + 3 \left\langle q_{(\mathbf{a}/\mathbf{a}, \mathbf{b}/\mathbf{b})} q_{(\mathbf{a}^2/\mathbf{a}, \mathbf{b}^2/\mathbf{b}^2)} \right\rangle_c - 3 \left\langle q_{(\mathbf{a}^3/\mathbf{a}^2, \mathbf{b}^3/\mathbf{b}^2)} \right\rangle_c + \left\langle q_{(\mathbf{a}^3/\mathbf{a}, \mathbf{b}^3/\mathbf{b})} \right\rangle_c \\ &= C_3^{\text{corr}}(\boldsymbol{\alpha}, \boldsymbol{\beta}; \boldsymbol{\alpha}, \boldsymbol{\beta}), \end{aligned} \quad (31)$$

where $C_k^{\text{corr}}(\varepsilon_m; \varepsilon_c)$ denotes the C_k corrected with the ε_c from the cumulants of $q_{(\alpha, \beta)}$ measured with the ε_m .

During the efficiency correction with another set of efficiency α' and β' , the detector efficiency α and β in the formulae of the relations between $\langle Q_{(\alpha, \beta)}^k Q_{(\alpha', \beta')}^l \rangle_c$ and $\langle q_{(\alpha, \beta)}^k q_{(\alpha', \beta')}^l \rangle_c$ are replaced with α' and β' , respectively, such as $C_k^{\text{corr}}(\alpha, \beta; \alpha', \beta')$. The following subsections will discuss the corrections by using the efficiency with the same averaged value as the detector efficiency but with different non-uniformity.

B. Internally averaged efficiency correction

In this subsection, the validity of the efficiency correction is studied by using an average of the detector efficiency within each single phase space, in other words, the average is not obtained across multiple phase spaces, which is called the internally averaged efficiency (IAE). Note that the average could be taken in parts of the bins divided from the phase spaces.

For example, the efficiency employed in the correction is set to

$$\alpha' = (\bar{\alpha}, \dots, \bar{\alpha}, \alpha_{m+1}, \dots, \alpha_M), \quad (32)$$

$$\beta' = (\bar{\beta}, \dots, \bar{\beta}, \beta_{n+1}, \dots, \beta_N), \quad (33)$$

with

$$\bar{\alpha} = \frac{\sum_{i=1}^m \langle x_i \rangle}{\sum_{i=1}^m} = \frac{\sum_{i=1}^m \alpha_i \langle X_i \rangle}{\sum_{i=1}^m} = \frac{\sum_{i=1}^m \alpha_i p_i}{\sum_{i=1}^m p_i}, \quad (34)$$

$$\bar{\beta} = \frac{\sum_{j=1}^n \langle y_j \rangle}{\sum_{j=1}^n} = \frac{\sum_{j=1}^n \beta_j \langle Y_j \rangle}{\sum_{j=1}^n} = \frac{\sum_{j=1}^n \beta_j q_j}{\sum_{j=1}^n q_j} \quad (35)$$

as the average of the detector efficiency α or β in the first m or n bins of a single phase space, respectively. One can find that

$$\frac{\alpha_i}{\alpha'_i} = \begin{cases} \frac{\alpha_i}{\bar{\alpha}}, & i = 1, 2, \dots, m \\ 1, & i = m+1, m+2, \dots, M \end{cases} \quad (36)$$

$$\frac{\beta_j}{\beta'_j} = \begin{cases} \frac{\beta_j}{\bar{\beta}}, & j = 1, 2, \dots, n \\ 1, & j = n+1, n+2, \dots, N \end{cases} \quad (37)$$

and

$$\sum_{i=1}^m \frac{\alpha_i}{\alpha'_i} p_i = \sum_{i=1}^m p_i \quad (38)$$

$$\sum_{j=1}^n \frac{\beta_j}{\beta'_j} q_j = \sum_{j=1}^n q_j. \quad (39)$$

If the particle charges are the same in all of the bins where the detector efficiency is averaged, that is, $a_1 = a_2 = \dots = a_m$ and $b_1 = b_2 = \dots = b_n$, it can be derived that

$$\begin{aligned} & \bar{\partial}_{(\alpha/\alpha', \beta/\beta')} \tilde{K}_f(s, t) \\ &= \bar{\partial}_{(\alpha\alpha/\alpha', \beta\beta/\beta')} \tilde{K}_f(s, t) \\ &= \left(\sum_{i=1}^M \frac{a_i \alpha_i}{\alpha'_i} p_i \frac{\partial}{\partial s} + \sum_{j=1}^N \frac{b_j \beta_j}{\beta'_j} q_j \frac{\partial}{\partial t} \right) K_f(s, t) \\ &= \left(\sum_{i=1}^M a_i p_i \frac{\partial}{\partial s} + \sum_{j=1}^N b_j q_j \frac{\partial}{\partial t} \right) K_f(s, t) \\ &= \bar{\partial}_{(\alpha, \beta)} \tilde{K}_f(s, t) \\ &= \bar{\partial}_{(\alpha/\alpha', \beta/\beta')} \tilde{K}_f(s, t) \end{aligned} \quad (40)$$

and so forth,

$$\begin{aligned} \langle Q_{(\alpha, \beta)}^k Q_{(\alpha', \beta')}^l \rangle_{\text{fc}} &= \langle q_{(\alpha/\alpha', \beta/\beta')}^k q_{(\alpha', \beta')}^l \rangle_{\text{fc}} \\ &= \langle q_{(\alpha/\alpha', \beta/\beta')}^k q_{(\alpha', \beta')}^l \rangle_{\text{fc}}, \end{aligned} \quad (41)$$

which denotes that the IAE α' and β' can also be employed to reproduce the factorial cumulants and even be converted into cumulants as well as the true detector efficiency α and β . As a check, $C_k^{\text{corr}}(\alpha, \beta; \alpha', \beta') = C_k^{\text{true}}$ if all of the α and β in Eqs. (29)-(31) are replaced with α' and β' , respectively. Thus, the IAE correction should be valid unless the average of the detector efficiency is taken for particles with different charges.

C. Externally averaged efficiency correction

In this subsection, the validity of the externally averaged efficiency (EAE) correction is further discussed by using an average of the detector efficiency across multiple phase spaces.

Simply, the particles with the same charge $a = b = 1$ are considered and each phase space is divided into one bin with $M = N = 1$. The efficiency correction applies the average of the detector efficiency across two phase spaces as

$$\bar{\varepsilon} = \frac{\langle x \rangle + \langle y \rangle}{\langle X \rangle + \langle Y \rangle} = \frac{\alpha \langle X \rangle + \beta \langle Y \rangle}{\langle X \rangle + \langle Y \rangle}. \quad (42)$$

By replacing the true detector efficiency in Eq. (29) with the EAE, the first-order cumulant is corrected with

$$\begin{aligned} C_1^{\text{corr}}(\alpha, \beta; \bar{\varepsilon}, \bar{\varepsilon}) &= \left\langle \frac{1}{\bar{\varepsilon}} x + \frac{1}{\bar{\varepsilon}} y \right\rangle_{\text{fc}} = \left\langle \frac{\alpha}{\bar{\varepsilon}} X + \frac{\beta}{\bar{\varepsilon}} Y \right\rangle_{\text{fc}} \\ &= \langle X + Y \rangle_{\text{c}} = C_1^{\text{true}}, \end{aligned} \quad (43)$$

which shows a successful correction for the first-order cumulant. However, for the second-order cumulant in the same way, the correction is obtained by

$$\begin{aligned}
C_2^{\text{corr}}(\alpha, \beta; \bar{\varepsilon}, \bar{\varepsilon}) &= \left\langle \left(\frac{1}{\bar{\varepsilon}}x + \frac{1}{\bar{\varepsilon}}y \right)^2 \right\rangle_{\text{fc}} + \left\langle \frac{1}{\bar{\varepsilon}}x + \frac{1}{\bar{\varepsilon}}y \right\rangle_{\text{fc}} \\
&= \left\langle \left(\frac{\alpha}{\bar{\varepsilon}}X + \frac{\beta}{\bar{\varepsilon}}Y \right)^2 \right\rangle_{\text{fc}} + \left\langle \frac{\alpha}{\bar{\varepsilon}}X + \frac{\beta}{\bar{\varepsilon}}Y \right\rangle_{\text{fc}} \\
&= \left\langle \left(\frac{\alpha}{\bar{\varepsilon}}X + \frac{\beta}{\bar{\varepsilon}}Y \right)^2 \right\rangle_{\text{c}} + \left\langle \left(\frac{\alpha}{\bar{\varepsilon}} - \frac{\alpha^2}{\bar{\varepsilon}^2} \right)X + \left(\frac{\beta}{\bar{\varepsilon}} - \frac{\beta^2}{\bar{\varepsilon}^2} \right)Y \right\rangle_{\text{c}} \\
&\not\equiv \langle (X + Y)^2 \rangle_{\text{c}} = C_2^{\text{true}}, \tag{44}
\end{aligned}$$

which is valid only in a few specific cases, such as that the detector efficiency $\alpha = \beta = 1$, that X and Y follow the multinomial distribution (a single phase space) and that X and Y follow two independent Poisson distributions ($C_1 = C_2 = \dots$). The corrections for higher-order cumulants are similar to the second-order case. In general, the EAE can not reproduce the cumulants higher than the first order.

D. Non-averaged efficiency correction

In this subsection, the validity of the efficiency correction is studied by using the non-averaged efficiency (NAE), which is defined by the efficiency with:

- different non-uniformity from the averaged efficiency,
- different non-uniformity from the detector efficiency,
- the same averaged value as the detector efficiency.

First, only one phase space is considered ($Y \equiv 0$), which is divided into two bins with $M = 2$. The particles with the same charge $a_1 = a_2 = 1$ are considered. The NAE employed in the correction is marked by $\boldsymbol{\alpha}' = (\alpha'_1, \alpha'_2)$, whose averaged value keeps the same as the detector efficiency as

$$\alpha = \frac{\alpha_1 \langle X_1 \rangle + \alpha_2 \langle X_2 \rangle}{\langle X_1 \rangle + \langle X_2 \rangle} = \frac{\alpha'_1 \langle X_1 \rangle + \alpha'_2 \langle X_2 \rangle}{\langle X_1 \rangle + \langle X_2 \rangle}, \tag{45}$$

and the efficiency can be rephrased with

$$\alpha_1 = \alpha - h \langle X_2 \rangle, \tag{46}$$

$$\alpha_2 = \alpha + h \langle X_1 \rangle, \tag{47}$$

$$\alpha'_1 = \alpha - h' \langle X_2 \rangle, \tag{48}$$

$$\alpha'_2 = \alpha + h' \langle X_1 \rangle. \tag{49}$$

The NAE correction for the first-order cumulant is ex-

pressed by

$$\begin{aligned}
C_1^{\text{corr}}(\boldsymbol{\alpha}; \boldsymbol{\alpha}') &= \left\langle \frac{x_1}{\alpha'_1} + \frac{x_2}{\alpha'_2} \right\rangle_{\text{c}} \\
&= \left\langle \frac{\alpha_1}{\alpha'_1} X_1 + \frac{\alpha_2}{\alpha'_2} X_2 \right\rangle_{\text{c}} \\
&= \left\langle \frac{\alpha - h \langle X_2 \rangle}{\alpha - h' \langle X_2 \rangle} X_1 + \frac{\alpha + h \langle X_1 \rangle}{\alpha + h' \langle X_1 \rangle} X_2 \right\rangle_{\text{c}} \\
&= \langle X_1 + X_2 \rangle_{\text{c}} \left(1 + \frac{h' (h' - h) \langle X_1 \rangle \langle X_2 \rangle}{(\alpha + h' \langle X_1 \rangle)(\alpha - h' \langle X_2 \rangle)} \right) \\
&\not\equiv \langle X_1 + X_2 \rangle_{\text{c}} = C_1^{\text{true}}, \tag{50}
\end{aligned}$$

which is valid only if $h' = 0$, $h' = h$ or $\langle X_1 \rangle \langle X_2 \rangle = 0$. The cases $h' = 0$ and $h' = h$ represent the efficiency corrections using the averaged efficiency and the true detector efficiency, respectively, rather than the NAE. If $\langle X_1 \rangle \langle X_2 \rangle = 0$, there is only one bin in the phase space, which does not meet the requirement $M = 2$. The corrections for higher-order cumulants are also invalid.

Second, two phase spaces are considered with $a = b = 1$ and $M = N = 1$. The averaged values of the detector efficiency and the NAE α' and β' are the same as

$$\bar{\varepsilon} = \frac{\alpha \langle X \rangle + \beta \langle Y \rangle}{\langle X \rangle + \langle Y \rangle} = \frac{\alpha' \langle X \rangle + \beta' \langle Y \rangle}{\langle X \rangle + \langle Y \rangle}. \tag{51}$$

The efficiency correction is also invalid in the same way, for example,

$$C_1^{\text{corr}}(\alpha, \beta; \alpha', \beta') \not\equiv C_1^{\text{true}}. \tag{52}$$

With the above two cases considered, the true values of cumulants could not be reproduced by the efficiency correction with the NAE.

III. TOY MODEL ANALYSIS WITH INTERNALLY AVERAGED EFFICIENCY

In this section, a toy Monte Carlo model with several sets of IAE with various non-uniformity is employed to check the theoretical derivation in the previous section and study the effect of the non-uniformity of the track efficiency applied in the correction on the cumulants up to fourth-order.

A. Event production

We produce 10^7 events with the numbers of positively and negatively charged particles (N_{pos} and N_{neg}) with the charges $a = 1$ and $b = -1$ following two independent Poisson distributions

$$N_{\text{pos}} \sim \text{Poisson}(\lambda_1), \tag{53}$$

$$N_{\text{neg}} \sim \text{Poisson}(\lambda_2), \tag{54}$$

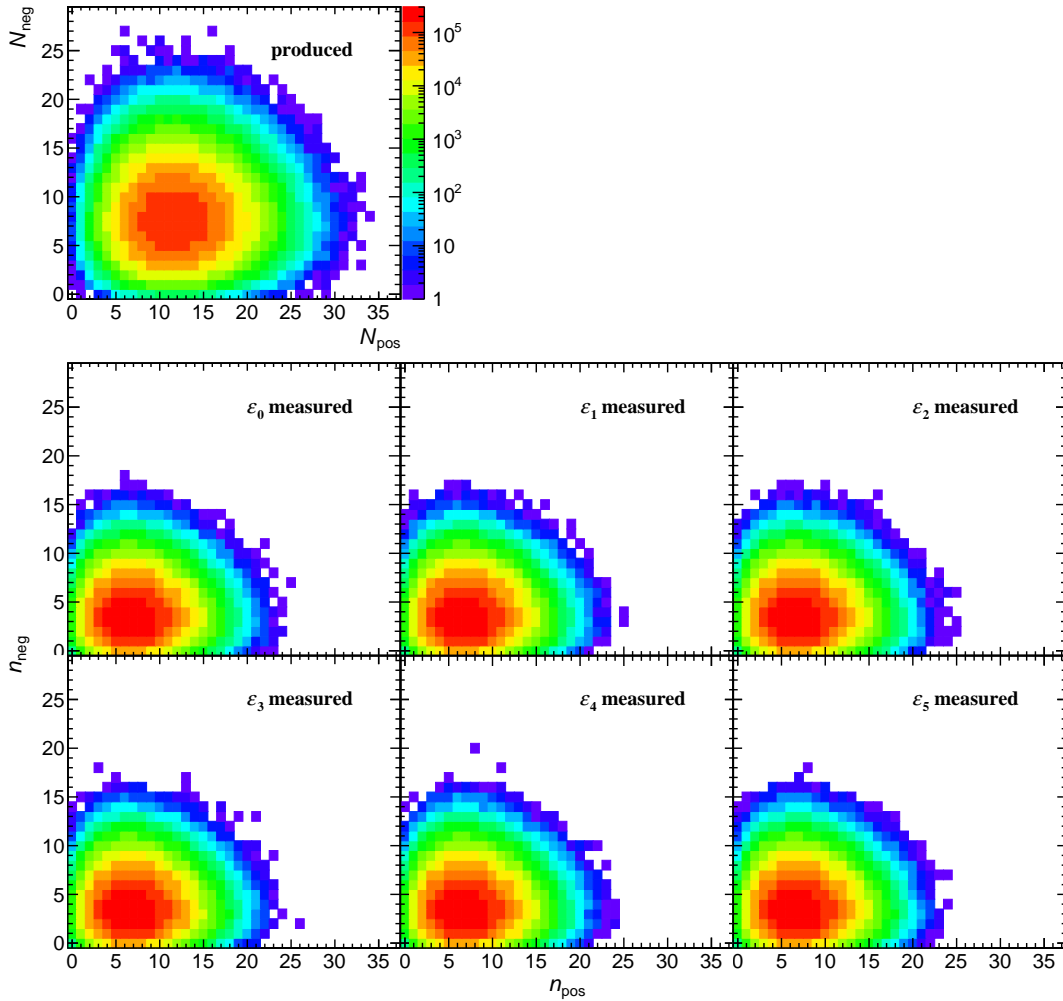


FIG. 1. (Color online) Correlations of produced and measured numbers of positively and negatively charged particles. The top panel shows the produced distribution, and others show the distributions measured with ε_i ($i = 0, 1, \dots, 5$) defined in Eqs. (64)-(69), respectively. Due to the equivalence of the averaged values of the efficiency, the measured distributions show indistinguishable.

where $\lambda_1 = 12$ and $\lambda_2 = 8$. The 2D plot of N_{pos} and N_{neg} is shown in the top panel of Fig. 1. There are two phase spaces made up by two types of particles, respectively, since the particle multiplicities do not follow a multinomial distribution.

Thus, the produced net-charge N_{net} ($= N_{\text{pos}} - N_{\text{neg}}$) follows the Skellam distribution [29]

$$N_{\text{net}} \sim \text{Skellam}(\lambda_1, \lambda_2), \quad (55)$$

and the theoretical cumulants up to fourth-order can be calculated as

$$C_1^{N_{\text{net}}} = C_3^{N_{\text{net}}} = \lambda_1 - \lambda_2, \quad (56)$$

$$C_2^{N_{\text{net}}} = C_4^{N_{\text{net}}} = \lambda_1 + \lambda_2. \quad (57)$$

Each of the particles in the produced events is allocated p_{T} and φ sampled from

$$f(p_{\text{T}}) \sim p_{\text{T}} \exp(-p_{\text{T}}/t), 0.4 \leq p_{\text{T}} < 2, \quad (58)$$

$$g(\varphi) \sim \text{Uniform}(0, 2\pi), \quad (59)$$

where $t = 0.26$ and 0.22 for positively and negatively charged particles, respectively. Distributions of the produced p_{T} and φ are shown as black curves in Fig. 2.

B. Efficiency definition

The track efficiency is considered, for example, to be p_{T} -and- φ -dependent as a two-dimensional function. Two independent one-dimensional components of efficiency are defined as

$$u(p_{\text{T}}) = p_0 \exp(-(p_1/p_{\text{T}})^{p_2}), \quad (60)$$

where $(p_0, p_1, p_2) = (0.7, 0.4, 4.8)$ for positively and $(0.6, 0.4, 4.2)$ for negatively charged particles, respectively,

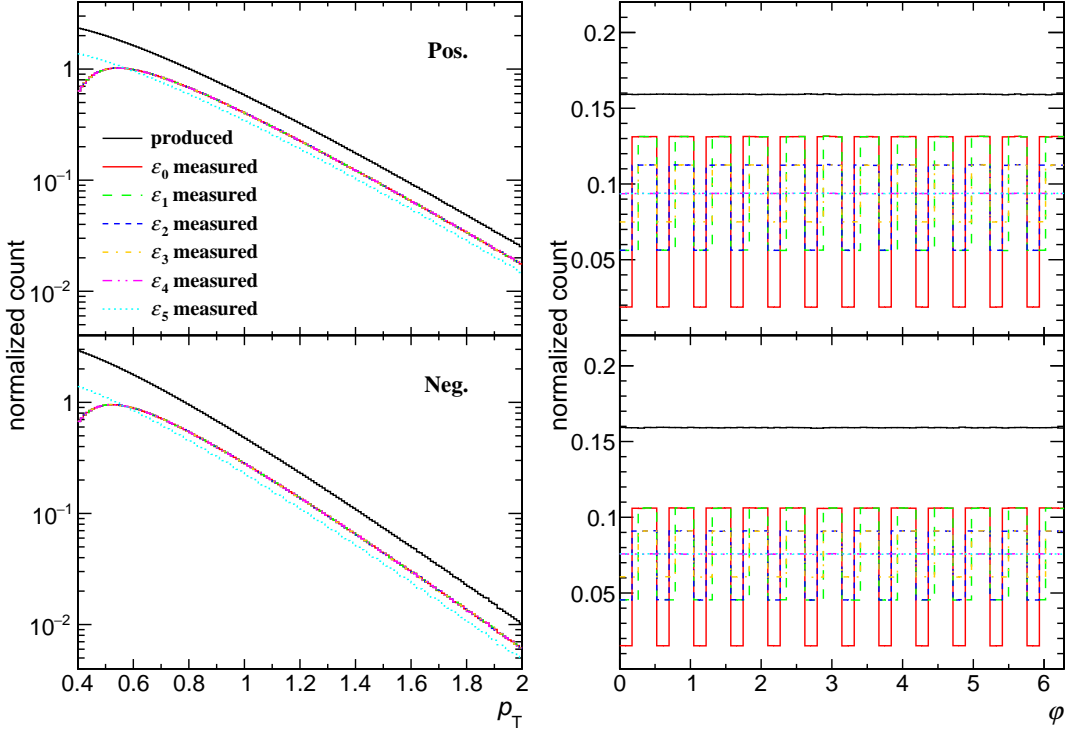


FIG. 2. (Color online) Distributions of produced and measured p_T and φ of positively (top) and negatively (bottom) charged particles. The produced p_T and φ distributions are shown as black curves, and the colored ones represent the distributions measured with ε_i ($i = 0, 1, \dots, 5$) defined in Eqs. (64)-(69), respectively. The measured p_T distributions with ε_i ($i = 0, 1, \dots, 4$) show indistinguishable due to their same $u(p_T)$ components, and with the same $v(\varphi)$, the measured φ distributions with ε_4 and ε_5 are almost overlapped.

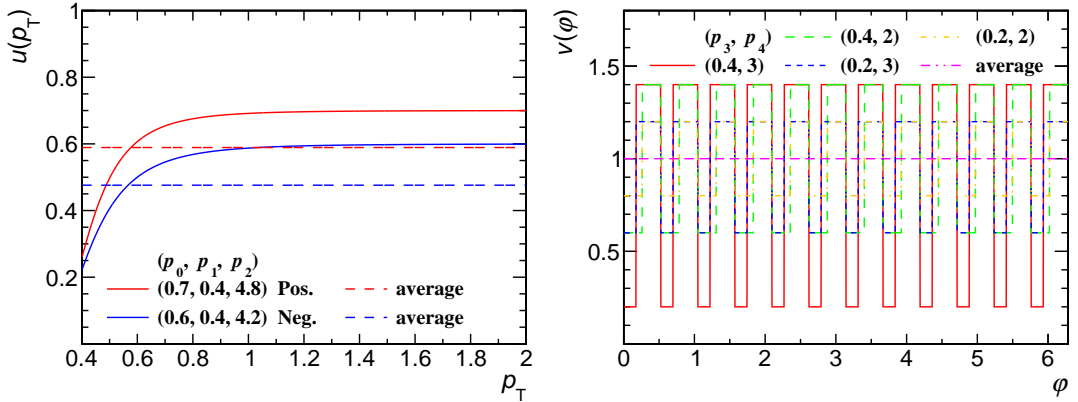


FIG. 3. (Color online) Two independent one-dimensional functions $u(p_T)$ and $v(\varphi)$ defined in Eqs. (60) and (61). The left panel shows $u(p_T)$ for positively and negatively charged particles as red and blue solid curves, respectively, and the right panel shows $v(\varphi)$ with various parameters as $(p_3, p_4) = (0.4, 3), (0.4, 2), (0.2, 3)$ and $(0.2, 2)$. Their averaged values defined in Eqs. (62) and (63) are also shown as horizontal dashed lines.

and

$$v(\varphi) = \begin{cases} 1 - p_3(p_4 - 1), & k \leq \varphi/\frac{\pi}{6} < k + \frac{1}{p_4}, \\ 1 + p_3, & k + \frac{1}{p_4} \leq \varphi/\frac{\pi}{6} < k + 1. \end{cases} \quad (61)$$

Figure 3 shows $u(p_T)$ for positively and negatively charged particles as solid curves in the left panel and $v(\varphi)$ with various parameters as $(p_3, p_4) = (0.4, 3), (0.4, 2), (0.2, 3)$ and $(0.2, 2)$ in the right panel. Their averaged values weighted by the input particle p_T or φ distribution

shown as horizontal dashed lines in Fig. 3 are defined as

$$\mu[u(p_T)] = \frac{\int_{0.4}^2 f(p_T) u(p_T) dp_T}{\int_{0.4}^2 f(p_T) dp_T}, \quad (62)$$

$$\mu[v(\varphi)] = \frac{\int_0^{2\pi} g(\varphi) v(\varphi) d\varphi}{\int_0^{2\pi} g(\varphi) d\varphi} \equiv 1, \quad (63)$$

respectively. There are 12 dips of $v(\varphi)$ with different widths as p_4 varies, which are proxies for the low efficiency in 12 φ bins due to the dead zone between every two adjacent Time Projection Chamber (TPC) sectors surrounding the heavy-ion beam [32].

Now six sets of track efficiency with different non-uniformity can be expressed as the products of Eqs. (60) and (61) given by

$$\varepsilon_0(p_T, \varphi) = u(p_T) v(\varphi), (p_3, p_4) = (0.4, 3), \quad (64)$$

$$\varepsilon_1(p_T, \varphi) = u(p_T) v(\varphi), (p_3, p_4) = (0.4, 2), \quad (65)$$

$$\varepsilon_2(p_T, \varphi) = u(p_T) v(\varphi), (p_3, p_4) = (0.2, 3), \quad (66)$$

$$\varepsilon_3(p_T, \varphi) = u(p_T) v(\varphi), (p_3, p_4) = (0.2, 2), \quad (67)$$

$$\varepsilon_4(p_T, \varphi) = u(p_T), \quad (68)$$

$$\varepsilon_5(p_T, \varphi) = \mu[u(p_T)], \quad (69)$$

whose averaged values and variances are defined as

$$\begin{aligned} \mu[\varepsilon_i(p_T, \varphi)] &= \frac{\int_{0.4}^2 \int_0^{2\pi} f(p_T) g(\varphi) \varepsilon_i(p_T, \varphi) dp_T d\varphi}{\int_{0.4}^2 \int_0^{2\pi} f(p_T) g(\varphi) dp_T d\varphi} \\ &= \mu[u(p_T)], \end{aligned} \quad (70)$$

$$\sigma^2[\varepsilon_i(p_T, \varphi)] = \mu[\varepsilon_i^2(p_T, \varphi)] - \mu^2[\varepsilon_i(p_T, \varphi)] \quad (71)$$

for $i = 0, 1, \dots, 5$, respectively. The μ and σ^2 of the efficiency are not the same for positively and negatively charged particles due to the different p_T distributions and different parameters of $u(p_T)$. Note that the averaged value of $\varepsilon_i(p_T, \varphi)$, $\mu[\varepsilon_i(p_T, \varphi)]$ keeps constant for $i = 0, 1, \dots, 5$. Statistical uncertainties of efficiency-corrected cumulants as a function of the averaged efficiency with a uniform distribution have been studied in Ref. [29]. Table I summarizes the σ^2/μ values quantifying the non-uniformity of various sets of efficiency. As i ($i = 0, 1, \dots, 5$) increases, the σ^2/μ of ε_i decreases monotonically to 0, which represents that ε_i becomes less non-uniform and that ε_5 is completely uniform.

C. Measurement and efficiency correction

Each particle in the produced events is sampled with six sets of track efficiency defined in Eqs. (64)-(69) as the

TABLE I. The σ^2/μ values of various sets of efficiency for positively and negatively charged particles.

Efficiency	Pos.	Neg.
ε_0	0.222	0.185
ε_1	0.123	0.105
ε_2	0.074	0.065
ε_3	0.050	0.045
ε_4	0.025	0.025
ε_5	0	0

probability, respectively. The 2D plots of the measured numbers of positively and negatively charged particles (n_{pos} and n_{neg}) are shown in Fig. 1, and the p_T and φ distributions are shown as colored curves in Fig. 2.

The so-called track-by-track efficiency corrections [31] with six sets of track efficiency are performed for each of the six measurements to obtain the $C_k^{\text{corr}}(\varepsilon_i; \varepsilon_j)$ ($i, j = 0, 1, \dots, 5$ and $k = 1, 2, 3, 4$). Note that the ε_c may not be the same as the ε_m .

The above procedures, including the measurement and the efficiency correction, are repeated 1000 times independently. The C_k^{corr} compared with the C_k^{true} are shown in Appendix A. Here the $\hat{\mu}$ and $\hat{\sigma}$ are defined as the mean value and the standard deviation of the C_k^{corr} , respectively, which can be found at the bottom of each panel of Figs. 12-17 in Appendix A. Figure 4 shows $\chi = (\hat{\mu} - C_k^{\text{true}})/\hat{\sigma}$ for various $(\varepsilon_m; \varepsilon_c)$, which quantifies the deviation of the C_k^{corr} from the C_k^{true} . For χ far away from ± 1 , it is drawn as a point at ± 1 with a red arrow pointing towards the larger value not shown within the y -axis scale, which denotes a failed efficiency correction. The point closest to 0 is pointed by two opposite red arrows, which indicates the best reproduction of the efficiency.

Figure 5 shows the fractions of the C_k^{corr} falling in between $C_k^{\text{true}} \pm \hat{\sigma}$ for various $(\varepsilon_m; \varepsilon_c)$, which are summarized from the number at the top right of each panel of Figs. 12-17 in Appendix A. All of the fractions of a successful efficiency correction should be comparable with 68% as the 1- σ probability of the Gaussian distribution.

Table II summarizes the successful and failed efficiency corrections for various $(\varepsilon_m; \varepsilon_c)$ differentiated by Figs. 4 and 5 and shows semi-diagonal. The simulated results support the theoretical predictions in the previous section. The diagonal line represents that the ε_c is the same as the ε_m and thus, the C_k^{true} can be recovered by the C_k^{corr} within uncertainties, which confirms that the track-by-track efficiency correction method is valid [31]. All of the successful efficiency correction at the bottom left of Table II employ the IAE of the ε_m as the ε_c . For example, ε_1 is the average of ε_0 in two φ bins, respectively,

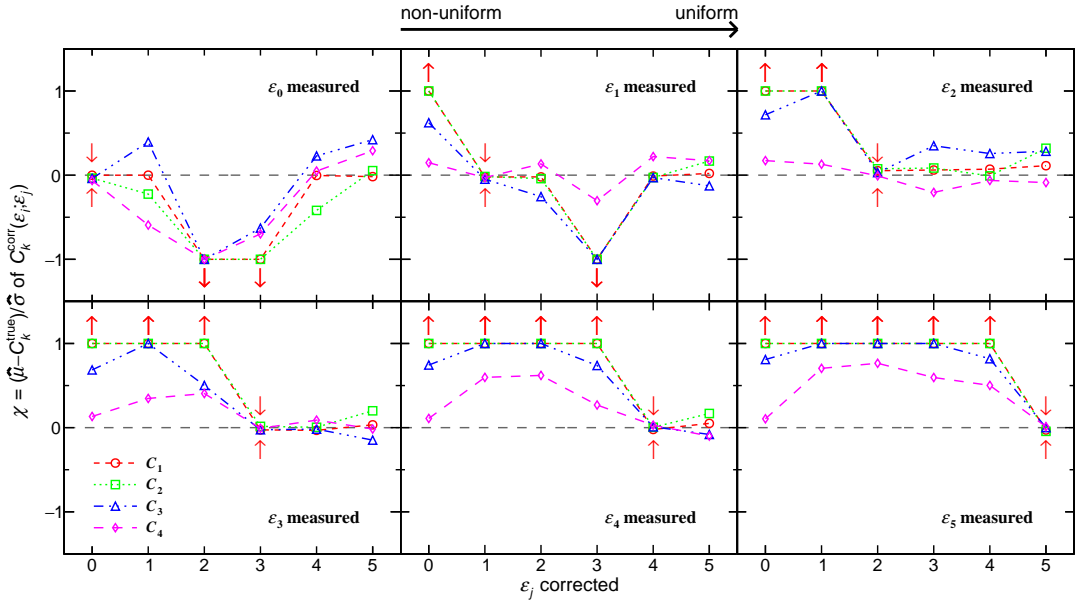


FIG. 4. (Color online) Quantified deviations $\chi = (\hat{\mu} - C_k^{\text{true}})/\hat{\sigma}$ ($k = 1, 2, 3, 4$) of the C_k^{corr} measured with ε_i and corrected with ε_j ($i, j = 0, 1, \dots, 5$) defined in Eqs. (64)-(69) from the C_k^{true} . For $|\chi| > 1$ of a failed efficiency correction, the point is drawn at ± 1 with a red arrow pointing towards the larger value not shown within the y -axis scale. The point pointed by two opposite red arrows represents the χ closest to 0.

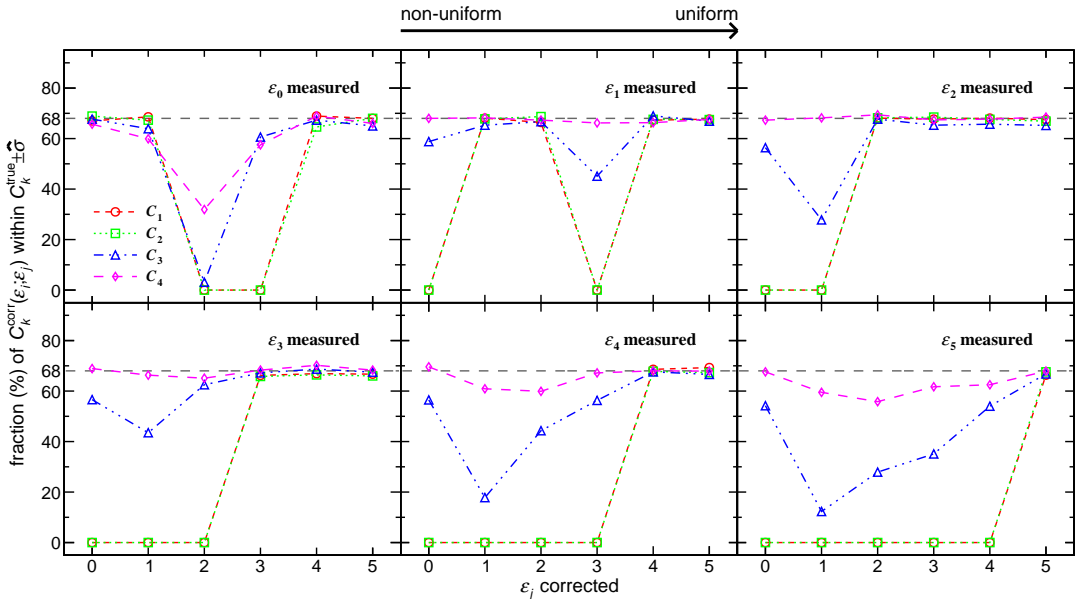


FIG. 5. (Color online) Fractions of the C_k^{corr} ($k = 1, 2, 3, 4$) measured with ε_i and corrected with ε_j ($i, j = 0, 1, \dots, 5$) defined in Eqs. (64)-(69) falling in between $C_k^{\text{true}} \pm \hat{\sigma}$. The fractions for the cumulants up to fourth-order obtained by each successful efficiency correction should be comparable with 68%.

as

$$\varepsilon_1(p_T, \varphi) = \begin{cases} \frac{\int_{k\pi/6}^{(k+1/2)\pi/6} g(\varphi) \varepsilon_0(p_T, \varphi) d\varphi}{\int_{k\pi/6}^{(k+1/2)\pi/6} g(\varphi) d\varphi}, & (k \in \mathbb{Z}) \\ \varepsilon_0(p_T, \varphi), & k + \frac{1}{2} \leq \varphi / \frac{\pi}{6} < k + 1, \end{cases} \quad (72)$$

so the correction with ε_1 can be performed successfully for the measurement with ε_0 . In the same way, ε_4 is the average of $\varepsilon_{0,1,2,3}$ in the whole φ range ($0 \leq \varphi < 2\pi$) and thus, ε_4 can be employed to correct the cumulants measured with $\varepsilon_{0,1,2,3}$. However, $\varepsilon_{2,3}$ (ε_3) could not be considered as the IAE of ε_0 (ε_1) but the NAE actually, which causes three “ \times ” at the bottom left of Table II. The effi-

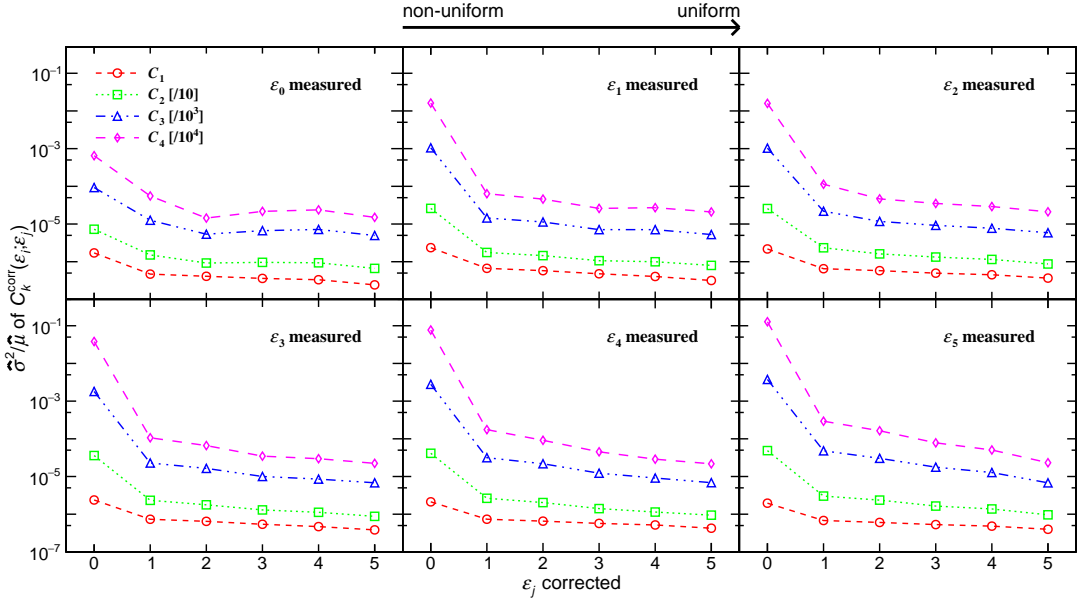


FIG. 6. (Color online) $\hat{\sigma}^2/\hat{\mu}$ of the C_k^{corr} ($k = 1, 2, 3, 4$) measured with ε_i and corrected with ε_j ($i, j = 0, 1, \dots, 5$) defined in Eqs. (64)-(69). The values quantify the statistical fluctuations and show a decreasing trend as the non-uniformity of ε_c decreases.

ciency corrections by using ε_c with more non-uniformity than ε_m at the top right of Table II also fails for the same reason. Once a non-averaged distribution is induced in the ε_c compared to the ε_m due to incorrect knowledge of the detector acceptance, it could not reproduce the cumulants and results in a failed correction. During the efficiency correction, we should safely take care of the internally averaged track efficiency and avoid introducing additional non-uniformity and non-averaged distributions. However, the statistical uncertainties should be treated carefully as what is studied in the followings.

TABLE II. The successful (\circ) and failed (\times) efficiency corrections for various sets of efficiency employed in measurement (ε_m) and correction (ε_c).

ε_m	ε_0	ε_1	ε_2	ε_3	ε_4	ε_5
ε_c	ε_0	ε_1	ε_2	ε_3	ε_4	ε_5
ε_0	\circ	\times	\times	\times	\times	\times
ε_1	\circ	\circ	\times	\times	\times	\times
ε_2	\times	\circ	\circ	\times	\times	\times
ε_3	\times	\times	\circ	\circ	\times	\times
ε_4	\circ	\circ	\circ	\circ	\circ	\times
ε_5	\circ	\circ	\circ	\circ	\circ	\circ

Figure 6 shows $\hat{\sigma}^2/\hat{\mu}$ for various $(\varepsilon_m; \varepsilon_c)$, which quantify the fluctuations of the C_k^{corr} and strongly relate to their statistical uncertainties. After removing three points of the failed efficiency corrections for $C_k^{\text{corr}}(\varepsilon_0; \varepsilon_2)$, $C_k^{\text{corr}}(\varepsilon_0; \varepsilon_3)$ and $C_k^{\text{corr}}(\varepsilon_1; \varepsilon_3)$, the decreasing trend shows that the statistical fluctuations and uncertainties of the C_k^{corr} are dramatically suppressed by the valid averaged efficiency corrections with less non-uniformity. In order to quantify how the statistical fluctuations are sup-

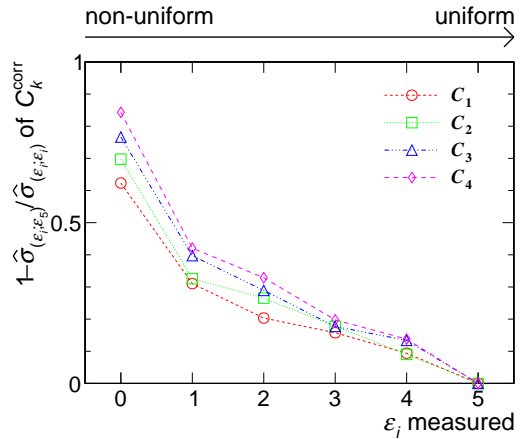


FIG. 7. (Color online) $1 - \hat{\sigma}_{(\varepsilon_i; \varepsilon_5)} / \hat{\sigma}_{(\varepsilon_i; \varepsilon_i)}$ of the efficiency-corrected cumulants up to fourth-order for various measurements with ε_i ($i = 0, 1, \dots, 5$) defined in Eqs. (64)-(69), where $\hat{\sigma}_{(\varepsilon_i; \varepsilon_j)}$ represents the $\hat{\sigma}$ of the cumulants measured with ε_i and corrected with ε_j ($j = i, 5$). The values quantify the suppression of the statistical uncertainties by the uniform efficiency correction and follow a decreasing trend as the non-uniformity of the efficiency employed in the measurement decreases.

pressed by the completely uniform efficiency correction, Fig. 7 summarizes $1 - \hat{\sigma}_{(\varepsilon_i; \varepsilon_5)} / \hat{\sigma}_{(\varepsilon_i; \varepsilon_i)}$ for various ε_m , where $\hat{\sigma}_{(\varepsilon_i; \varepsilon_5)}$ and $\hat{\sigma}_{(\varepsilon_i; \varepsilon_i)}$ denote the $\hat{\sigma}$ of $C_k^{\text{corr}}(\varepsilon_i; \varepsilon_5)$ and $C_k^{\text{corr}}(\varepsilon_i; \varepsilon_i)$ ($i = 0, 1, \dots, 5$), respectively. In the uniform efficiency correction with ε_5 , the non-uniformity of the track efficiency is ignored, which could farthest flatten the fluctuations and minimize the statistical un-

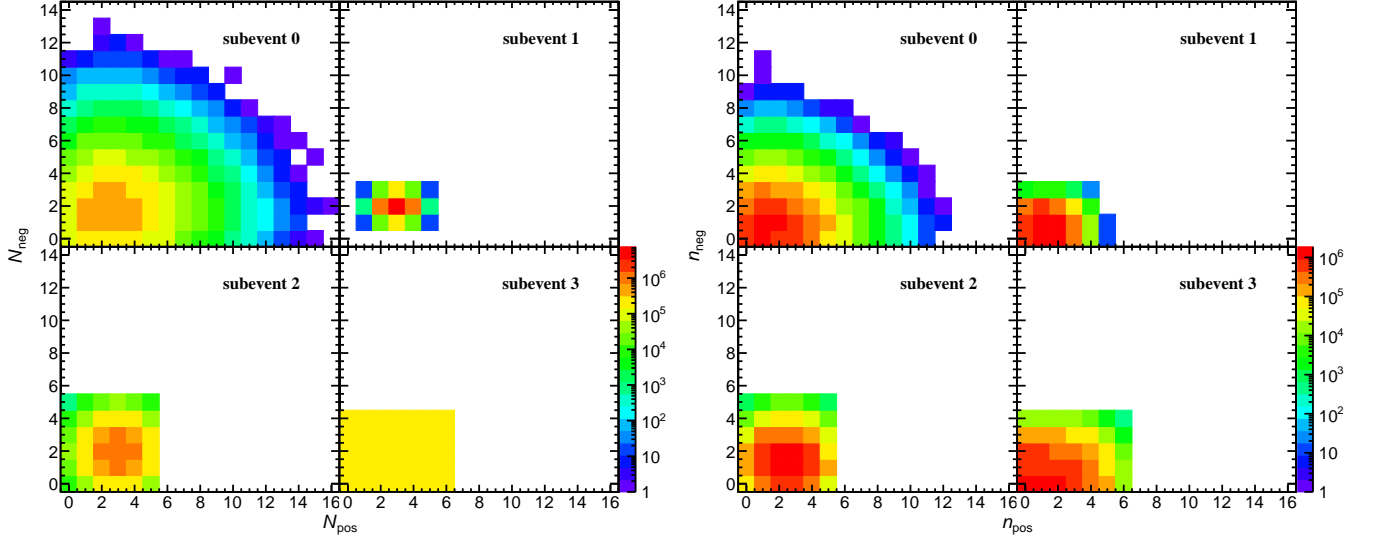


FIG. 8. (Color online) Correlations of produced and measured numbers of positively and negatively charged particles in various subevents. The left panels show the produced distributions, and the right ones show the distributions measured with ε_0 defined in Eq. (77).

certainties.

In addition, another sample of events are produced with N_{pos} and N_{neg} following Gaussian distributions as well and the above procedures are repeated. Similar results are obtained and show independence of the input particle multiplicity distributions.

IV. TOY MODEL ANALYSIS WITH EXTERNALLY AVERAGED EFFICIENCY

In this section, another toy Monte Carlo model with EAE is further employed in order to check the previous theoretical study about the validity of the EAE correction.

A. Event production

We produce 10^7 events with positively and negatively charged particles with the charges $a = 1$ and $b = -1$. Four subevents are divided in each event according to the particle p_T and φ in various intervals. The multiplicities of two types of particles in four subevents are sampled independently and thus, there are eight phase spaces accordingly. Table III summarizes the subevent divisions and the N_{pos} and N_{neg} distributions in four subevents. Note that the total numbers of particles are the same in different subevents, since the averaged multiplicities $\langle N_{\text{pos}} \rangle \equiv 3$ and $\langle N_{\text{neg}} \rangle \equiv 2$ keep constant. The 2D plots of N_{pos} and N_{neg} in various subevents are shown in the left panels of Fig. 8.

Each of the particles in each subevent is allocated p_T

TABLE III. Subevent divisions and distributions of N_{pos} and N_{neg} in four subevents.

	$0 \leq \varphi < \pi$	$\pi \leq \varphi < 2\pi$
$0.4 \leq p_T < 0.8$	subevent 0 $N \sim \text{Poisson}(\lambda)$	subevent 1 $N \sim \text{Gaus}(\mu, \sigma)$
$0.8 \leq p_T < 2$	subevent 2 $N \sim \text{Binomial}(n, p)$	subevent 3 $N \sim \text{Integer}(n_{\text{max}})^*$

* integer uniformly distributed on the interval $[0, n_{\text{max}} - 1]$

$\lambda = 3$ (pos), 2 (neg)

$(\mu, \sigma) = (3, 0.4)$ (pos), $(2, 0.25)$ (neg)

$(n, p) = (5, 0.6)$ (pos), $(5, 0.4)$ (neg)

$n_{\text{max}} = 7$ (pos), 5 (neg)

and φ sampled from

$$f(p_T) \sim p_T \exp(-p_T/t), \quad (73)$$

$$g(\varphi) \sim \exp(-\varphi/\tau), \quad (74)$$

where $t = 0.26$ and 0.22 and $\tau = 8$ and 6 for positively and negatively charged particles, respectively. Distributions of the produced p_T and φ are shown as black solid curves in Fig. 9.

B. Efficiency definition

Two independent one-dimensional components of efficiency are defined as

$$u(p_T) = p_0 \exp(-(p_1/p_T)^{p_2}), \quad (75)$$

$$v(\varphi) = 1 + p_3 \sin(p_4 \varphi + p_5), \quad (76)$$

where $(p_0, p_1, p_2, p_3, p_4, p_5) = (0.7, 0.4, 4.8, 0.4, 1.2, -\pi/6)$ for positively and $(0.6, 0.4, 4.2, 0.4, 0.8, \pi/12)$

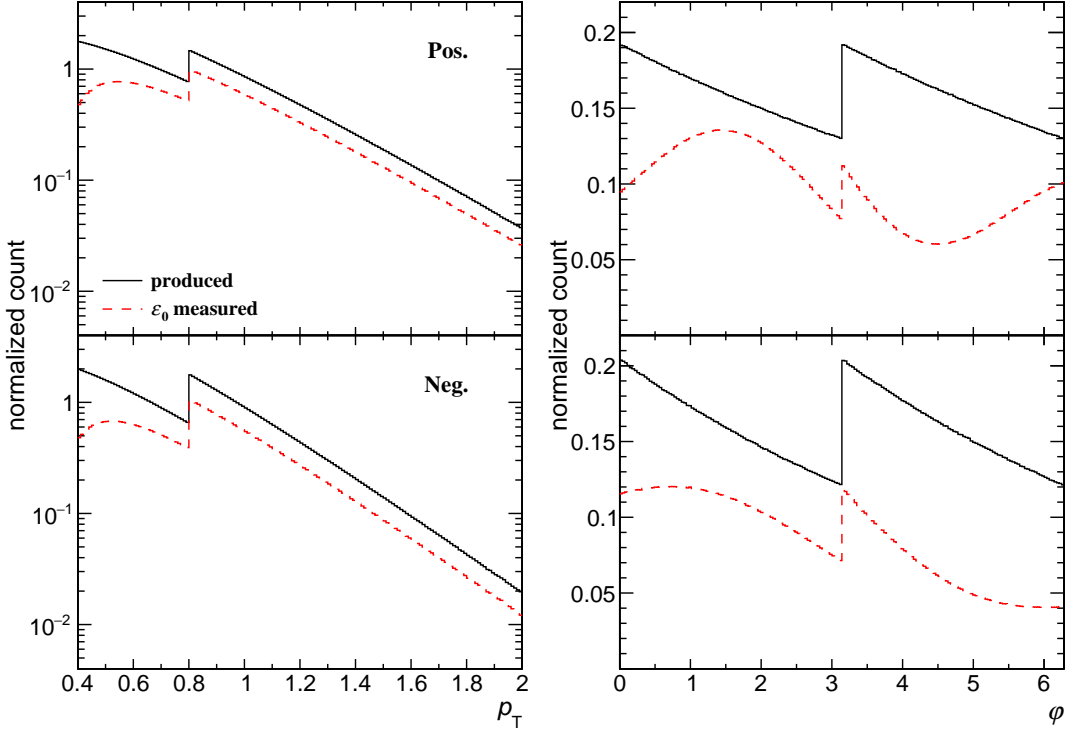


FIG. 9. (Color online) Distributions of produced and measured p_T and φ of positively (top) and negatively (bottom) charged particles. The produced p_T and φ distributions are shown as black solid curves, and the red dashed ones represent the distributions measured with ε_0 defined in Eq. (77). The steps at $p_T = 0.8$ and $\varphi = \pi$ are caused by sampling N_{pos} and N_{neg} from the input distributions individually in multiple phase spaces.

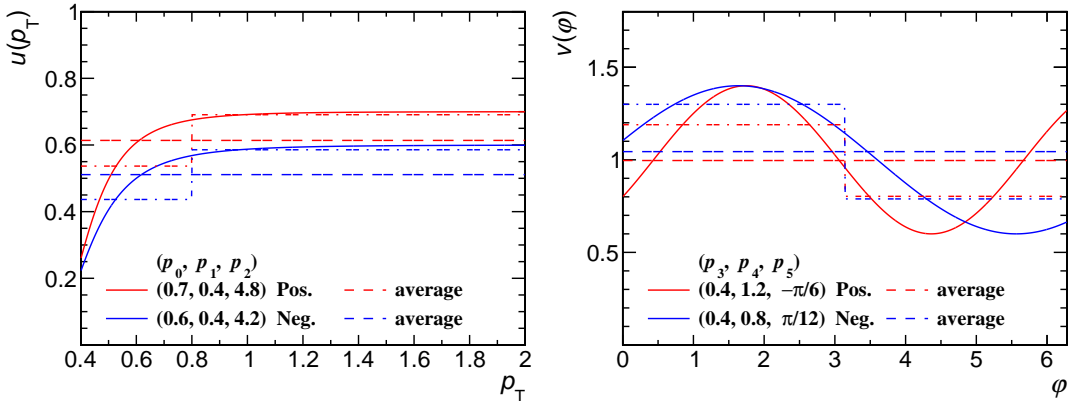


FIG. 10. (Color online) Two independent one-dimensional functions $u(p_T)$ and $v(\varphi)$ defined in Eqs. (75) and (76). The $u(p_T)$ and $v(\varphi)$ for positively and negatively charged particles are shown as red and blue solid curves, respectively, and the horizontal dashed lines denote their averaged values in $p_T \in [0.4, 0.8]$, $[0.8, 2]$ and $[0.4, 2]$ or $\phi \in [0, \pi]$, $[\pi, 2\pi]$ and $[0, 2\pi]$.

for negatively charged particles, respectively. Figure 10 shows these two functions and their averaged values weighted by the input particle p_T or φ distribution in $p_T \in [0.4, 0.8]$, $[0.8, 2]$ and $[0.4, 2]$ or $\phi \in [0, \pi]$, $[\pi, 2\pi]$ and $[0, 2\pi]$.

Three sets of track efficiency are given by

$$\varepsilon_0(p_T, \varphi) = u(p_T) v(\varphi), \quad (77)$$

$$\varepsilon_1(p_T, \varphi) = \mu[\varepsilon_0(p_T, \varphi)]_{\text{sub of } (p_T, \varphi)}, \quad (78)$$

$$\varepsilon_2(p_T, \varphi) = \mu[\varepsilon_0(p_T, \varphi)], \quad (79)$$

where $\mu[\varepsilon_0(p_T, \varphi)]_{\text{sub of } (p_T, \varphi)}$ denotes the average of ε_0 within the subevent in which the particle (p_T, φ) falls, so the ε_1 is defined as the IAE of ε_0 . However, the ε_2 represents the EAE as the average of ε_0 across four subevents.

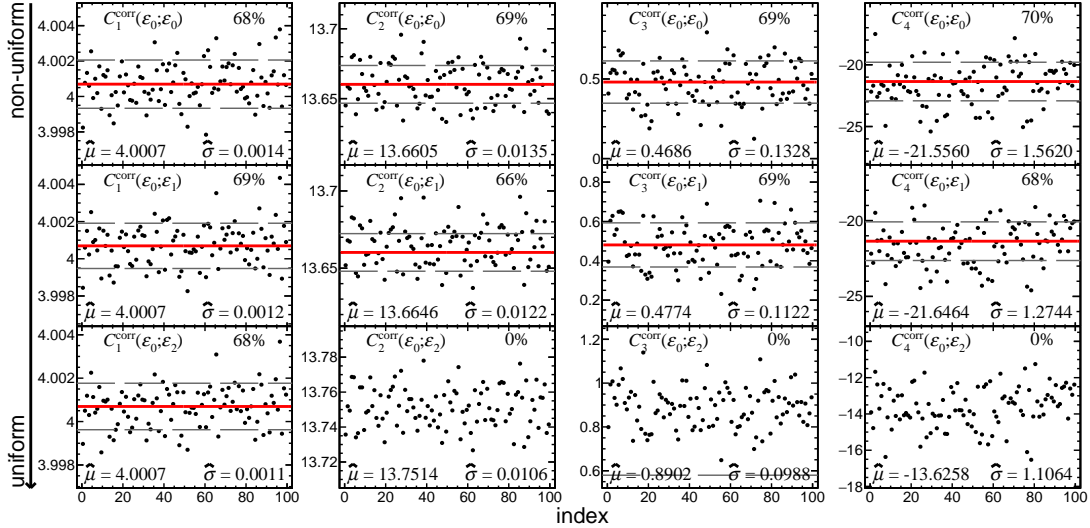


FIG. 11. (Color online) The C_k^{corr} ($k = 1, 2, 3, 4$) measured with ε_0 and corrected with each set of efficiency defined in Eqs. (77)-(79). Each panel shows 100 points instead of 1000 ones. The $\hat{\mu}$ and $\hat{\sigma}$ at the bottom of each panel show the mean value and the standard deviation of 1000 points. The red solid and gray dashed lines denote the C_k^{true} and $C_k^{\text{true}} \pm \hat{\sigma}$, respectively. The number at the top right of each panel represents the fraction of the points falling in between the gray dashed lines.

C. Measurement and efficiency correction

Each particle in the produced events is sampled with ε_0 defined in Eq. (77) as the probability and the track-by-track efficiency corrections [31] with three sets of track efficiency defined in Eqs. (77)-(79) are performed to obtain the $C_k^{\text{corr}}(\varepsilon_0; \varepsilon_j)$ ($j = 0, 1, 2$ and $k = 1, 2, 3, 4$). The 2D plots of n_{pos} and n_{neg} in four subevents are shown in the right panels of Fig. 8, and the p_{T} and φ distributions are shown as red dashed curves in Fig. 9.

The measurement and the efficiency correction are repeated 1000 times independently. The C_k^{corr} compared with C_k^{true} are shown in Fig. 11. The $\hat{\mu}$ and $\hat{\sigma}$ of 1000 points are shown at the bottom of each panel. The red solid lines represent the C_k^{true} , and the gray dashed lines denote $C_k^{\text{true}} \pm \hat{\sigma}$. The fraction of the C_k^{corr} falling in between the gray dashed lines is shown at the top right of each panel, which should be comparable with 68% for a valid efficiency correction. Figure 11 clearly shows that the C_k^{true} can be successfully reproduced by the efficiency correction with ε_1 for the measurement with ε_0 within uncertainties, which supports the validity of the IAE correction. However, there is no C_2 , C_3 or C_4 corrected with ε_2 falling in between the gray dashed lines in Fig. 11, in other words, the efficiency correction with the EAE could not reproduce the C_k^{true} for $k > 1$ within uncertainties, which has been predicted by the previous theoretical study. This indicates that the usage of averaged efficiency in the efficiency correction requires comprehensive knowledge about the phase space dependence and the EAE correction for higher-order cumulants should be avoided in the data analysis.

V. SUMMARY

In this paper, we investigate the effect of non-uniform track efficiency on the efficiency correction of higher-order cumulants of conserved charges. The theoretical study by tuning the track efficiency employed in the efficiency correction proves that the averaged efficiency within each single phase space could successfully reproduce the true values of cumulants if we avoid averaging the detector efficiency for particles with different charges. However, the efficiency correction with taking an average across multiple phase spaces or introducing a non-averaged distribution is invalid.

The toy model simulation with the track-by-track based efficiency correction supports the theoretical proof and shows that the statistical uncertainties of cumulants are strongly correlated with the non-uniformity of the valid efficiency correction applied. The averaged efficiency correction with a uniform detector acceptance results in a significant suppression of the uncertainties since the event-by-event fluctuations of the efficiency from a non-uniform detector acceptance are not taken into account. However, the efficiency correction with the averaged efficiency across multiple phase spaces is not valid, which requires a comprehensive knowledge of different phase spaces when applying an averaged efficiency correction. If we safely use the realistic distribution of the detector acceptance in the efficiency correction, precisely understanding the cumulants of conserved charges with small uncertainties requires as uniform track efficiency as possible. The uniformity of the detector design and construction is crucial for fluctuation measurements in future facilities in lower energy and high baryon density region, such as NICA-MPD and FAIR-CBM.

ACKNOWLEDGMENTS

This work was partially supported by National Key Research and Development Program of China with Grant No. 2018YFE0205200, 2018YFE0104700, 2020YFE0202002, Natural Science Foundation of China

with Grant No. 11890712, 11828501, 11861131009, Anhui Provincial Natural Science Foundation with Grant No. 1808085J02 and Key Laboratory of Quark and Lepton Physics (MOE) at CCNU with Grant No. QLPL2020P01.

[1] L. D. McLerran, *Rev. Mod. Phys.* **58**, 1021 (1986).

[2] S. A. Bass, M. Gyulassy, H. Stoecker, and W. Greiner, *J. Phys. G* **25**, R1 (1999), arXiv:hep-ph/9810281.

[3] J. Adams *et al.* (STAR Collaboration), *Nucl. Phys. A* **757**, 102 (2005), arXiv:nucl-ex/0501009.

[4] K. Adcox *et al.* (PHENIX Collaboration), *Nucl. Phys. A* **757**, 184 (2005), arXiv:nucl-ex/0410003.

[5] B. Muller, J. Schukraft, and B. Wyslouch, *Ann. Rev. Nucl. Part. Sci.* **62**, 361 (2012), arXiv:1202.3233 [hep-ex].

[6] Y. Akiba *et al.*, arXiv:1502.02730 [nucl-ex].

[7] X. Luo, S. Shi, N. Xu, and Y. Zhang, *Particles* **3**, 278 (2020), arXiv:2004.00789 [nucl-ex].

[8] F. Si, X.-L. Chen, L. Zhou, Y.-F. Zhang, S.-H. Zhang, X.-Y. Ju, X.-J. Li, X. Dong, and N. Xu, *Phys. Lett. B* **805**, 135465 (2020), arXiv:1906.08974 [nucl-ex].

[9] L. Adamczyk *et al.* (STAR Collaboration), *Phys. Rev. Lett.* **118**, 212301 (2017), arXiv:1701.06060 [nucl-ex].

[10] Y. Aoki, G. Endrodi, Z. Fodor, S. D. Katz, and K. K. Szabo, *Nature* **443**, 675 (2006), arXiv:hep-lat/0611014.

[11] F. Karsch, *Nucl. Phys. A* **590**, 367C (1995), arXiv:hep-lat/9503010.

[12] P. de Forcrand and O. Philipsen, *Nucl. Phys. B* **642**, 290 (2002), arXiv:hep-lat/0205016.

[13] G. Endrodi, Z. Fodor, S. D. Katz, and K. K. Szabo, *JHEP* **04**, 001, arXiv:1102.1356 [hep-lat].

[14] P. Braun-Munzinger and J. Wambach, *Rev. Mod. Phys.* **81**, 1031 (2009), arXiv:0801.4256 [hep-ph].

[15] K. Fukushima and T. Hatsuda, *Rept. Prog. Phys.* **74**, 014001 (2011), arXiv:1005.4814 [hep-ph].

[16] S. Gupta, X. Luo, B. Mohanty, H. G. Ritter, and N. Xu, *Science* **332**, 1525 (2011), arXiv:1105.3934 [hep-ph].

[17] H.-T. Ding, F. Karsch, and S. Mukherjee, *Int. J. Mod. Phys. E* **24**, 1530007 (2015), arXiv:1504.05274 [hep-lat].

[18] M. A. Stephanov, K. Rajagopal, and E. V. Shuryak, *Phys. Rev. D* **60**, 114028 (1999), arXiv:hep-ph/9903292.

[19] S. Ejiri, F. Karsch, and K. Redlich, *Phys. Lett. B* **633**, 275 (2006), arXiv:hep-ph/0509051.

[20] M. A. Stephanov, *Phys. Rev. Lett.* **102**, 032301 (2009), arXiv:0809.3450 [hep-ph].

[21] M. Asakawa, S. Ejiri, and M. Kitazawa, *Phys. Rev. Lett.* **103**, 262301 (2009), arXiv:0904.2089 [nucl-th].

[22] M. A. Stephanov, *Phys. Rev. Lett.* **107**, 052301 (2011), arXiv:1104.1627 [hep-ph].

[23] X. Li, F. Si, Z. Fu, and Y. Zhang, *Nucl. Phys. Rev.* **36**, 395 (2019).

[24] X. Luo, *Nucl. Phys. A* **956**, 75 (2016), arXiv:1512.09215 [nucl-ex].

[25] X. Luo (STAR Collaboration), *PoS CPOD2014*, 019 (2015), arXiv:1503.02558 [nucl-ex].

[26] J. Adam *et al.* (STAR), *Phys. Rev. Lett.* **126**, 092301 (2021).

[27] M. Abdallah *et al.* (STAR Collaboration), arXiv:2101.12413 [nucl-ex].

[28] X. Luo, *J. Phys. G* **39**, 025008 (2012), arXiv:1109.0593 [physics.data-an].

[29] X. Luo, *Phys. Rev. C* **91**, 034907 (2015), arXiv:1410.3914 [physics.data-an].

[30] A. Pandav, D. Mallick, and B. Mohanty, *Nucl. Phys. A* **991**, 121608 (2019), arXiv:1809.08892 [nucl-ex].

[31] X. Luo and T. Nonaka, *Phys. Rev. C* **99**, 044917 (2019), arXiv:1812.10303 [physics.data-an].

[32] M. Anderson *et al.*, *Nucl. Instrum. Meth. A* **499**, 659 (2003), arXiv:nucl-ex/0301015.

[33] M. M. Aggarwal *et al.* (STAR Collaboration), *Phys. Rev. Lett.* **105**, 022302 (2010), arXiv:1004.4959 [nucl-ex].

[34] L. Adamczyk *et al.* (STAR Collaboration), *Phys. Rev. Lett.* **112**, 032302 (2014), arXiv:1309.5681 [nucl-ex].

[35] T. Nonaka, M. Kitazawa, and S. Esumi, *Phys. Rev. C* **95**, 064912 (2017), [Erratum: *Phys. Rev. C* 103, 029901 (2021)], arXiv:1702.07106 [physics.data-an].

[36] M. Kitazawa and X. Luo, *Phys. Rev. C* **96**, 024910 (2017), arXiv:1704.04909 [nucl-th].

Appendix A

The C_k^{corr} ($k = 1, 2, 3, 4$) measured with ε_i and corrected with ε_j ($i, j = 0, 1, \dots, 5$) defined in Eqs. (64)-(69) are shown in Figs. 12-17. The $\hat{\mu}$ and $\hat{\sigma}$ shown at the bottom of each panel represent the mean value and the standard deviation of 1000 points, respectively. The red solid lines show the C_k^{true} and the gray dashed lines denote the C_k^{true} shifted up and down with the $\hat{\sigma}$ ($C_k^{\text{true}} \pm \hat{\sigma}$). The fraction of the C_k^{corr} falling in between the gray dashed lines is shown at the top right of each panel.

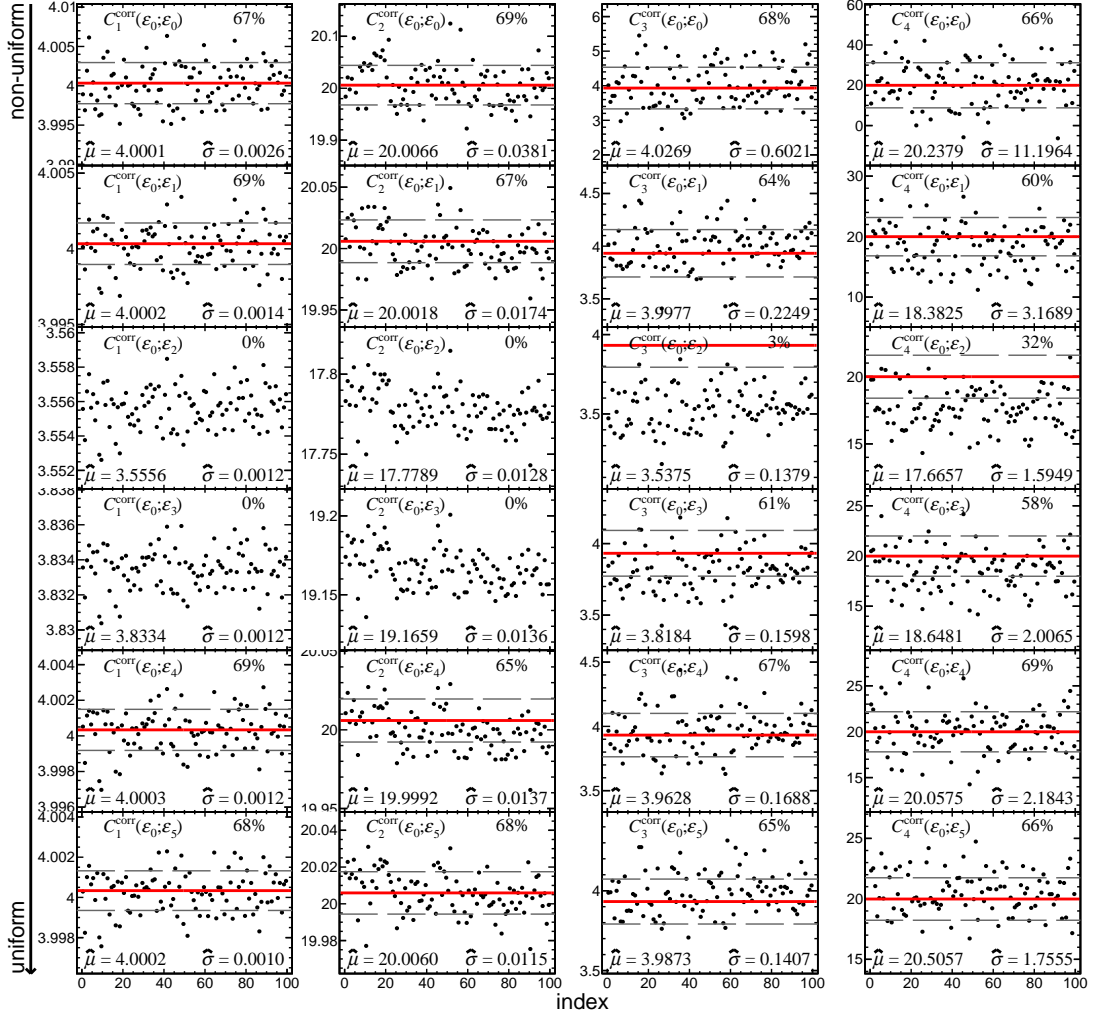


FIG. 12. (Color online) The C_k^{corr} ($k = 1, 2, 3, 4$) measured with ε_0 and corrected with each set of efficiency defined in Eqs. (64)-(69). Each panel shows 100 points instead of 1000 ones. The $\hat{\mu}$ and $\hat{\sigma}$ at the bottom of each panel show the mean value and the standard deviation of 1000 points. The red solid and gray dashed lines denote the C_k^{true} and $C_k^{\text{true}} \pm \hat{\sigma}$, respectively. The number at the top right of each panel represents the fraction of the points falling in between the gray dashed lines.

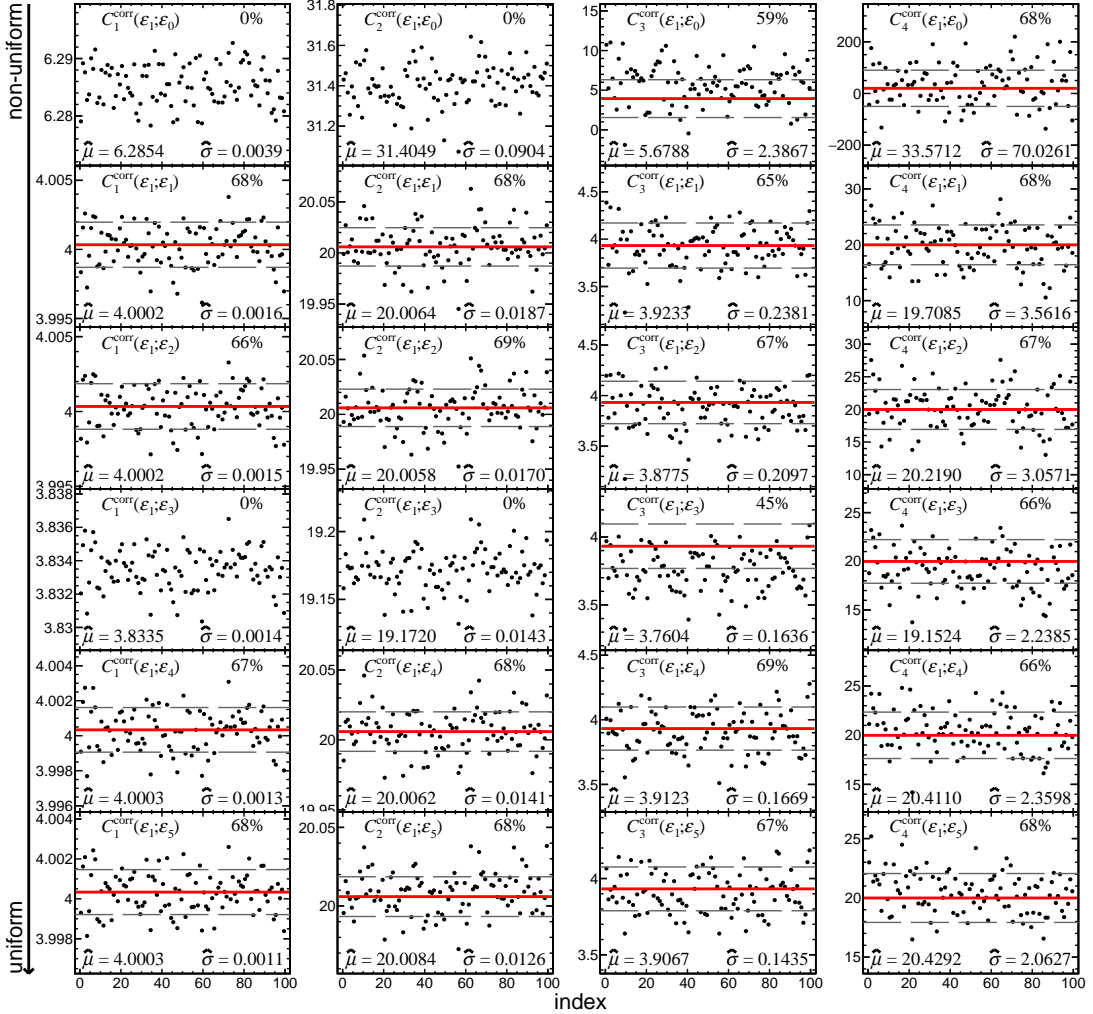


FIG. 13. (Color online) The C_k^{corr} ($k = 1, 2, 3, 4$) measured with ε_1 and corrected with each set of efficiency defined in Eqs. (64)-(69). Each panel shows 100 points instead of 1000 ones. The $\hat{\mu}$ and $\hat{\sigma}$ at the bottom of each panel show the mean value and the standard deviation of 1000 points. The red solid and gray dashed lines denote the C_k^{true} and $C_k^{\text{true}} \pm \hat{\sigma}$, respectively. The number at the top right of each panel represents the fraction of the points falling in between the gray dashed lines.

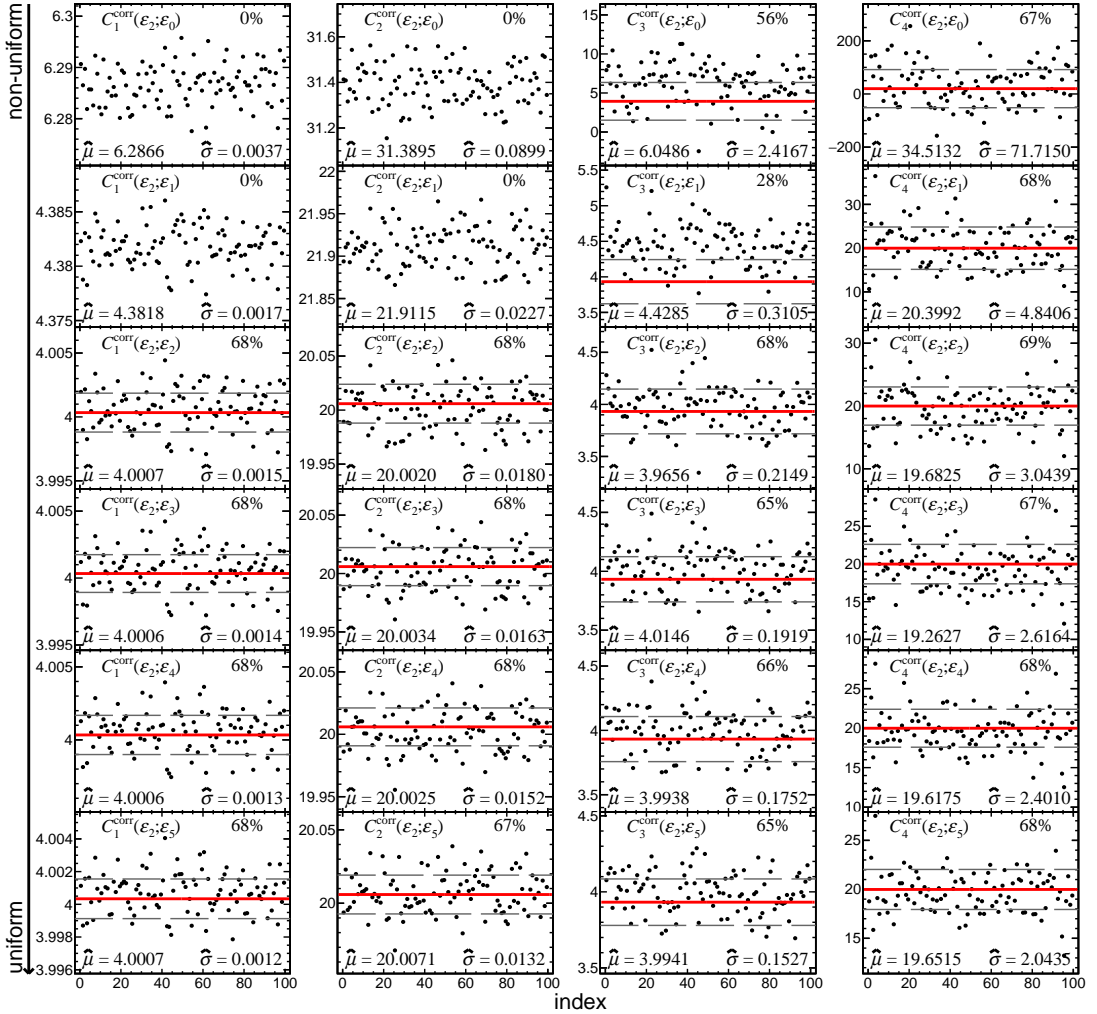


FIG. 14. (Color online) The C_k^{corr} ($k = 1, 2, 3, 4$) measured with ε_2 and corrected with each set of efficiency defined in Eqs. (64)-(69). Each panel shows 100 points instead of 1000 ones. The $\hat{\mu}$ and $\hat{\sigma}$ at the bottom of each panel show the mean value and the standard deviation of 1000 points. The red solid and gray dashed lines denote the C_k^{true} and $C_k^{\text{true}} \pm \hat{\sigma}$, respectively. The number at the top right of each panel represents the fraction of the points falling in between the gray dashed lines.

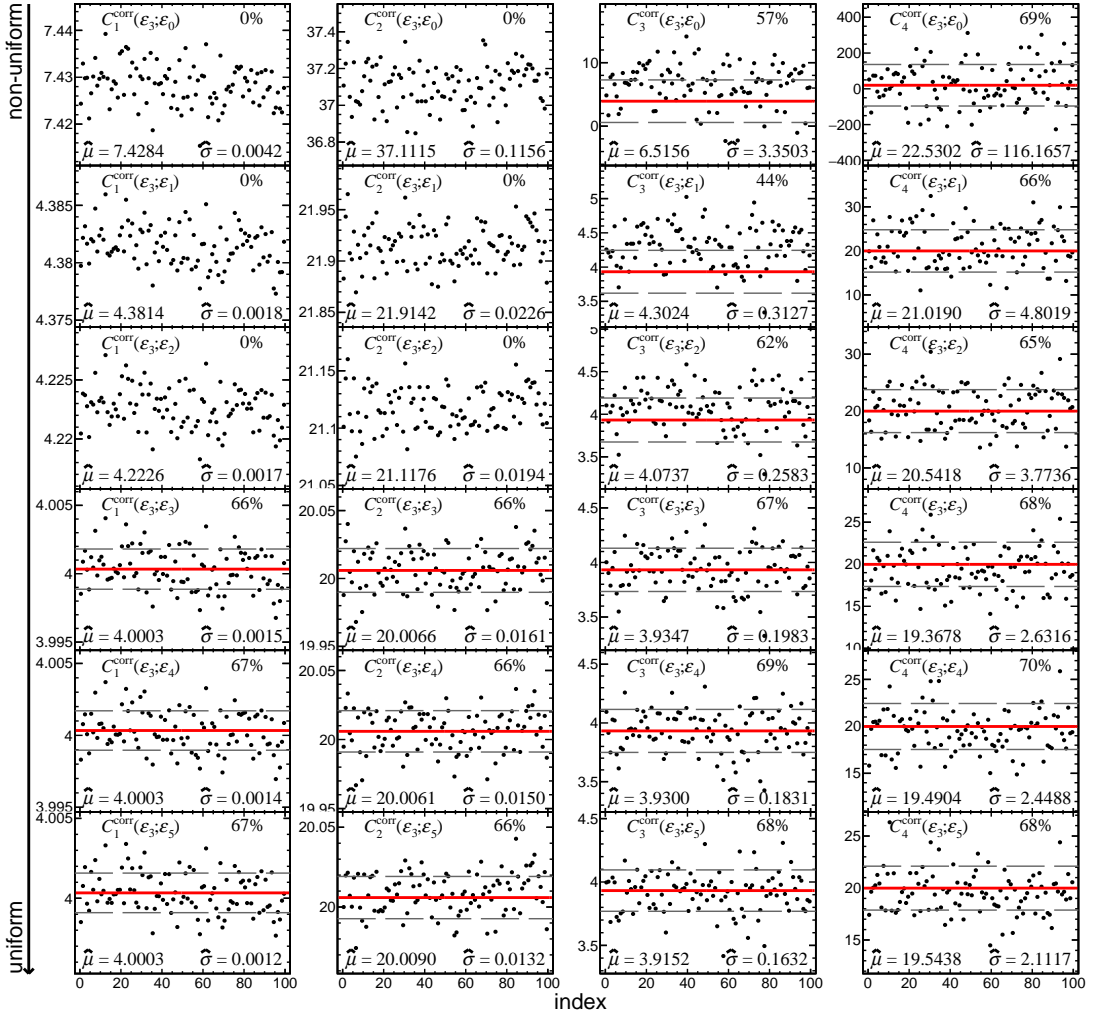


FIG. 15. (Color online) The C_k^{corr} ($k = 1, 2, 3, 4$) measured with ε_3 and corrected with each set of efficiency defined in Eqs. (64)-(69). Each panel shows 100 points instead of 1000 ones. The $\hat{\mu}$ and $\hat{\sigma}$ at the bottom of each panel show the mean value and the standard deviation of 1000 points. The red solid and gray dashed lines denote the C_k^{true} and $C_k^{\text{true}} \pm \hat{\sigma}$, respectively. The number at the top right of each panel represents the fraction of the points falling in between the gray dashed lines.

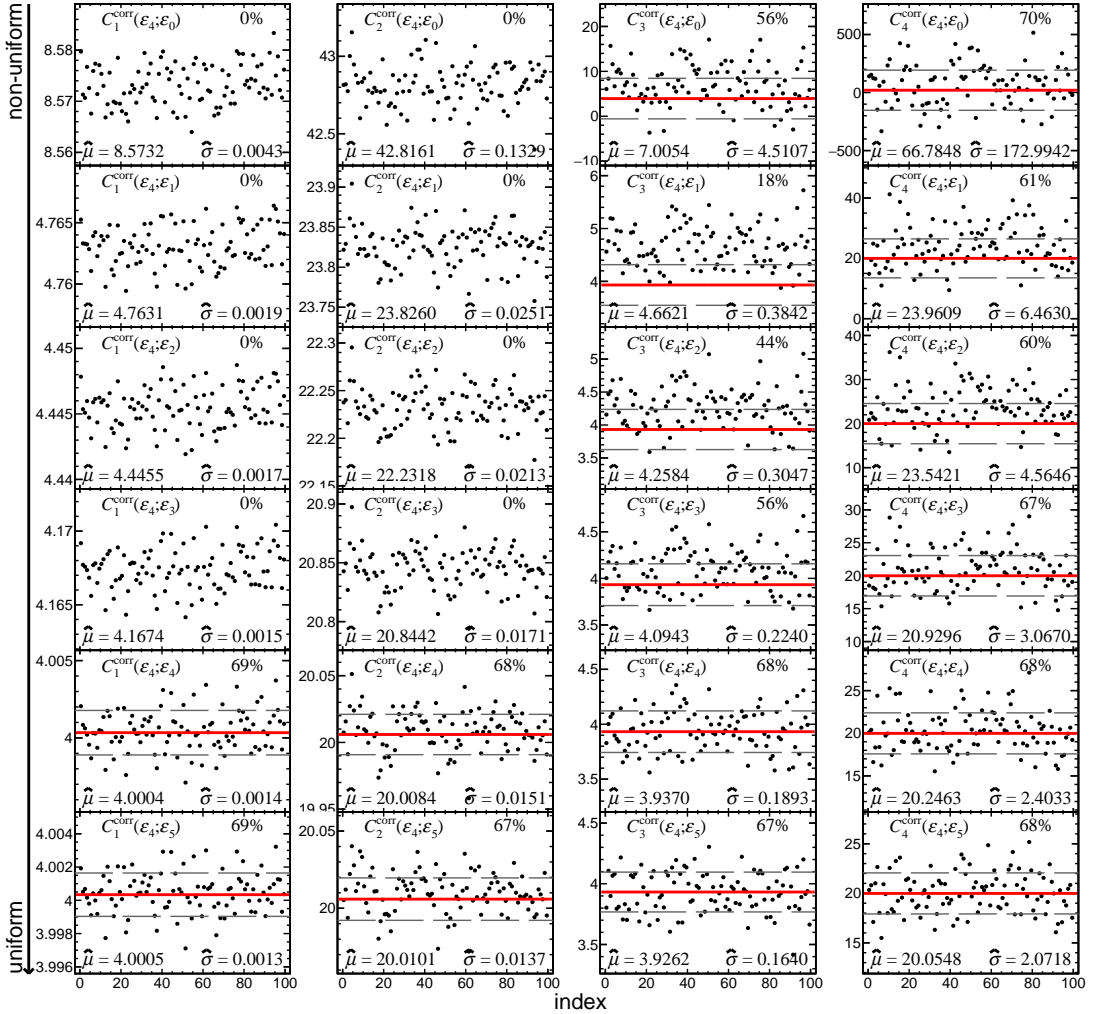


FIG. 16. (Color online) The C_k^{corr} ($k = 1, 2, 3, 4$) measured with ϵ_4 and corrected with each set of efficiency defined in Eqs. (64)-(69). Each panel shows 100 points instead of 1000 ones. The $\hat{\mu}$ and $\hat{\sigma}$ at the bottom of each panel show the mean value and the standard deviation of 1000 points. The red solid and gray dashed lines denote the C_k^{true} and $C_k^{\text{true}} \pm \hat{\sigma}$, respectively. The number at the top right of each panel represents the fraction of the points falling in between the gray dashed lines.

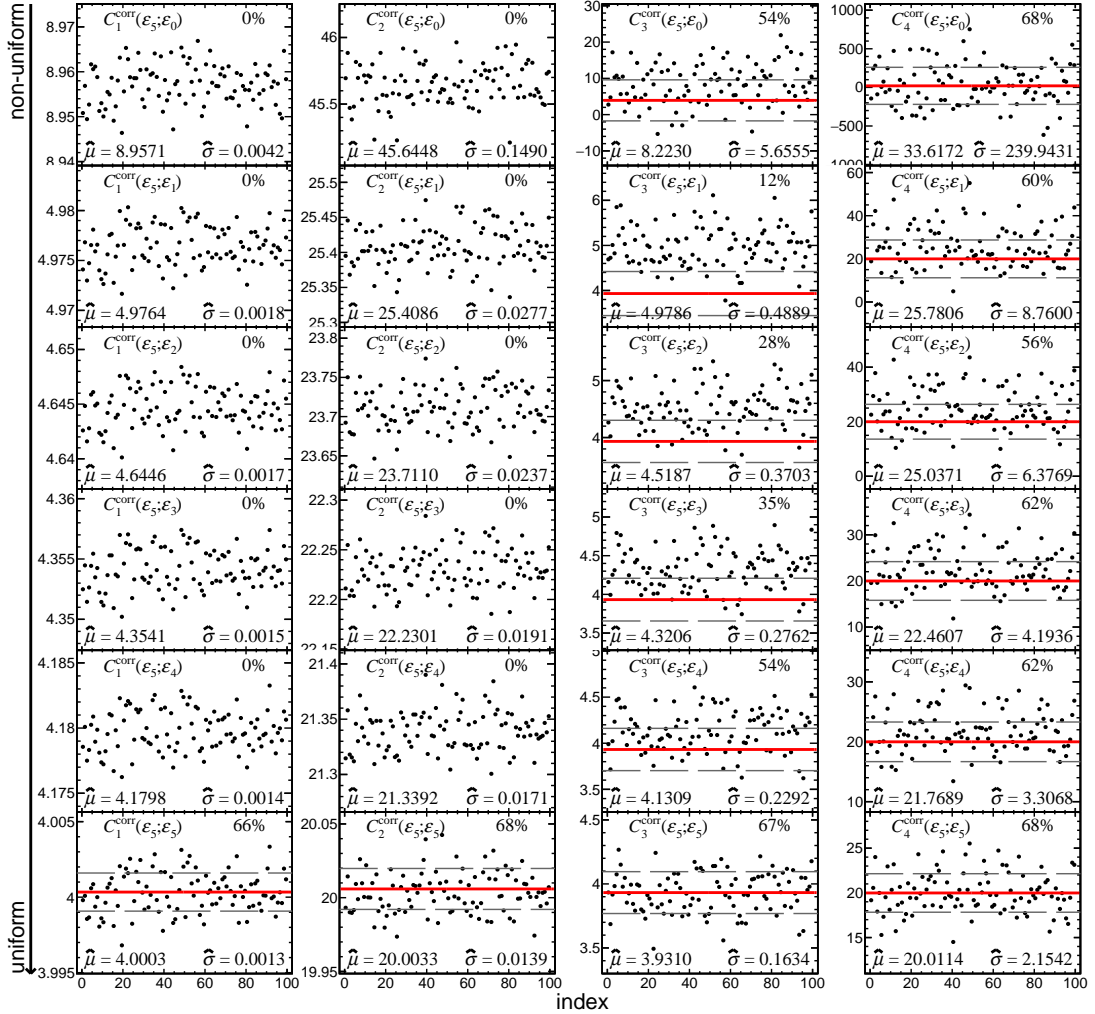


FIG. 17. (Color online) The C_k^{corr} ($k = 1, 2, 3, 4$) measured with ε_5 and corrected with each set of efficiency defined in Eqs. (64)-(69). Each panel shows 100 points instead of 1000 ones. The $\hat{\mu}$ and $\hat{\sigma}$ at the bottom of each panel show the mean value and the standard deviation of 1000 points. The red solid and gray dashed lines denote the C_k^{true} and $C_k^{\text{true}} \pm \hat{\sigma}$, respectively. The number at the top right of each panel represents the fraction of the points falling in between the gray dashed lines.